Diffraction-Based Method To Evaluate Enzymatic Degradation Of Polylactic Acid Films

by Valeria Amellalli Hernandez-Salgado

A thesis submitted in partial fulfillment of the requirements for the degree of

Master of Science

in

Materials Engineering

Department of Chemical and Materials Engineering

University of Alberta

Abstract

Commodity plastics fate has become one of the most critical environmental concerns. Due to their resistance to degradation, plastics are accumulating into a massive amount of waste on land and in water. These materials are harming the ecosystems. Among the several alternatives studied, biodegradable bio-sourced polymers like polylactic acid (PLA) have been considered a potential replacement for oil-based plastics. PLA is a biopolymer that is not only biocompatible, but it presents physical properties that can be used in several areas like drug delivery, food packaging, agriculture and polymer thin films.

Polymer thin films are used in applications in different areas. They can be used in microelectronics, functional coatings or optical components. Understanding degradation and stability are essential for their correct utilization. However, current characterization methods for the degradation of polymer thin films are mainly focus on gravimetric data. Polymer thin films present minuscule mass changes and these methods do not provide complete information about their stability. In this work, an optical technique that can be used to monitor the degradation of polymer thin films is explored. This technique was demonstrated previously in our group as a qualitative method to study the degradation of a semicrystalline biopolymer: polyhydroxybutyrate (PHB). In this technique, films are first patterned with a grating on their surface. The films are then immersed in degrading solutions under different conditions. During the immersion, a laser-irradiated the polymer surface, such that the grating diffracts the beam. A photodetector measures the beam intensity, and the degradation is monitored by observing the change in intensity of the first diffraction order spot.

In current work, this method is firstly used to compare the degradation of polylactic acid thin films in various environments. PLA is known for being degraded by hydrolysis, and the presence of an enzyme can accelerate its biodegradation. The intensity decreased as the polymer

is degraded by proteinase K. Atomic force microscope (AFM), images were collected at different degradation stages to determine the relationship between the PLA surface and the diffracted intensity. Optimized degradation conditions were identified using PLA films patterned with a triangular diffraction grating. These conditions were pH 8, 200 μg/mL and 37ºC. This method was also able to demonstrate the effect of changes in pH, temperature and enzyme concentration in the degradation rate.

The data obtained from the diffraction method allows *qualitative* comparisons of degradation rate, as shown by the change in intensity of the diffraction pattern over time. To extract *quantitative* information regarding etch rates from the intensity data collected using the optical diffraction method, a model was introduced in OmniSim software. This model provides the link between the intensity of the diffracted beam and the geometry of the grating. By applying the model, for the first time, it was possible to obtain quantitative information for polymer thin film degradation rates (nm/min) by measuring the diffraction intensity. The etch rate of this polymer thin film under optimum conditions, was 8.5 nm/min. By using gratings with different heights and cross-sectional profiles, the effect of different shapes on both the intensity and degradation rate was studied.

Using this technique, biopolymers can be considered in polymer thin film applications since their stability can now be evaluated with a sensitive method. In the same manner, applications of polymer thin films can be expanded to biomedical areas where biodegradability is necessary since this method can be applied under a variety of conditions. Thus, these results provide an alternative to evaluating polymer thin film degradation that provides quantitative information.

Preface

A segment of this work forms part of an international research collaboration, directed by Dr. Anastasia Elias at the University of Alberta, with Dr. Kenneth Harris at National Research Council Canada – Nanotechnology Research Centre and Mr. Fabian Goßler and Dr. Tobias Koenig at the Leibniz Institute of Polymer Research in Dresden, Germany.

Dr. Elias and Dr. Harris conceived the idea. Mr. Fabian Goßler fabricated the SU8 molds presented in Chapter 3. Dr. Harris conducted the simulations for the different grating shapes.

I was responsible for the literature review in Chapter 2, the modification to the setup referred to in Chapter 3, the data collection showed in Chapter 4 and the concluding analysis in Chapter 5.

Dr. Elias and Dr. Harris supervised the work and contributed to manuscript edits, conceptualization, and advice to data interpretation.

This thesis is dedicated to my husband,

my parents and my sister

who support me all this time.

Acknowledgments

I would like to thank my supervisors Dr. Anastasia Elias and Dr. Kenneth Harris, of the Department of Chemical and Materials Engineering (CME) at the University of Alberta and National Research Council Canada-Nanotechnology Research Centre. I really appreciate the opportunity to study under their supervision. They were always available to point me in the right direction and to discuss any questions of the research. This work would never happen without your acceptance, and for that, I am infinitely grateful.

I was fortunate to be able to interact with my colleagues from Elias research group. I am grateful for all the advice, training, feedback, comments and support showed during this journey. To NanoFab staff that helped me with the trainings and answered all my questions. All the analysis were possible because of their patience. I would like to acknowledge the financial support from Natural Sciences and Engineering Research Council of Canada (NSERC) that made this work possible.

A Ricardo, mi esposo, gracias por tu paciencia y valentía en esta aventura, por tus palabras tan certeras que siempre llegaron en el momento adecuado. Siempre me has motivado a arriesgarme y agradezco inmensamente esas alas. A mis papas, Martha Alicia y Miguel Ángel, y mi hermana Gaby, por impulsarme y creer en mí. Gracias por ser parte con sus consejos y bromas. Verlos siempre me dio fuerzas para seguir adelante y siempre pensé en ustedes como una guía. La ciencia es un camino lleno de curiosidad que me han enseñado, y por haberme inculcado ese interés, a ustedes les dedico este trabajo. A otros miembros de mi familia, les agradezco todo su cariño y alegría con la que siempre me recibieron. Desde mi abuelo Félix, Ángel, a mis tías y primos, sus consejos los atesoro.

To all my friends, I had the pleasure of meeting in Canada, Edher, Oileng and Liang, who were my family in Edmonton. To Jorge, Andres and the friends in the blue house for the infinite meetings just to catch up. To my very beloved Mexican friends, Ireri, Ivonne, Karla and Rudo, science people that always provided me with their immense support.

Table of Contents

List of tables

List of figures

List of abbreviations

ρ	Polymer density
σ	Tensile strength
E	Tensile modulus
ε	Ultimate strain
σ*	Specific tensile strength
E*	Specific tensile modulus
AcC	Acetyl cellulose
AFM	Atomic force microscopy
BOD	Biological oxygen demand
DNA	Deoxyribonucleic acid
DSC	Differential scanning calorimetry
DTA	Differential thermal analysis
FTIR	Fourier transform infrared
GPC	Gel permeation chromatography
M_w	Molecular weight
NMR	Nuclear magnetic resonance
NY11	Nylon 11
PBS	Polybutylene succinate
PCL	Polycaprolactone
PDLA	Poly(D-lactide)
PDLLA	poly(DL-lactide)
PDMS	Polydimethylsiloxane
PE	Polyethylene
PET	Polyethylene terephthalate
PHB	Polyhrydroxybutyrate
PLA	Polylactic acid
PLLA	Poly(L-lactide)
PP	Polypropylene
PS	Polystyrene

PVC	Polyvinyl chloride
QCM	Quartz crystal microbalance
RCWA	Rigorous coupled-wave analysis
SEM	Scanning electron microscopy
SPR	Surface Plasmon resonance
T_g	Glass transition temperature
T_m	Melting temperature
TGA	Thermogravimetric analysis
TMM	Triangular master mold
TOD	Theoretical oxygen demand
UV	Ultraviolet
XPS	X-ray photoelectron spectroscopy
XRD	X-ray diffraction

1. Introduction

Throughout history, humans have been influenced by materials. Materials have marked specific stages, including the Stone Age (until 2500 BC), the Bronze Age (~2500-700 BC), and the Iron Age (700 BC-100 AD) [1]. Some are calling our current times the "Plastic Age" [2].

In the latter half of the last century, polymers derived from petroleum products have added convenience to our lives. These materials are undeniably useful, and their characteristics are attractive for multiple applications. For example, plastics represent an option to reduce fuel usage as lightweight components for cars and airplanes [2]. They can form inexpensive objects by casting, and plastics are used as sterile dressings in medical applications [2]. Nowadays, plastics are present in almost all our activities as they are lightweight and have excellent barrier properties, flexibility, strength, corrosion resistance, and low cost [2]. However, today, the most common use of plastic is as disposable packaging, which is discarded within a year of production [3]. It has been estimated that by 2017, 8,300 million metric tons of plastic had been produced in the world [4]. Of the total plastic produced, only 9% is in circulation as recycled material, while 79% is in landfills, and 12% has been incinerated [4]. Every minute, one million plastic bags are used, and the majority are made from oil-based traditional polymers [5]. This massive production of petroleum-based synthetic polymers, along with these polymers' durability and resistance to degradation has led to a specific problem: plastic waste accumulation [3].

The massive production of plastic is not necessarily a problem, but its use in packaging, which is discarded after just minutes of use, leads to an enormous accumulation of waste. Features like durability and degradation resistance were once considered to be benefits; however, now, they are a major disadvantage since the degradation time of oil polymers extends to hundreds of years [6]. Moreover, inappropriate disposal strategies (such as incineration) avoid any assimilation by nature [4]. When plastics are incinerated, the release of plasticizer compounds into the atmosphere creates adverse environmental effects [4]. A popular alternative is recycling, but this is only a partial solution. Even when recycling can reduce oil usage, carbon dioxide emissions, and water consumption, recycling methods are limited, and recycled plastics generally have diminished properties [7]. New chemical advances are still needed to increase

the quantity of recycled plastic waste [7]. The lack of effective strategies to manage plastic waste has led to an exaggerated introduction of industrial waste products into the ecosystem [8].

Plastic waste production, so-called “white pollution”, threatens to become a public health problem since much of the discarded plastic inadvertently ends up in the oceans [5], [9]. Because most plastic cannot break down chemically, oceanic plastic waste can only be mechanically eroded. These small fragments, generally known as “microplastics”, are already found in oceans, estuaries, bodies of freshwater and arctic ice [10]. The accumulated plastic waste is now oceanic debris affecting marine animals and sea birds [11].

The potentially disastrous consequences emphasize the importance of finding a solution to an imminent problem. In the search for an answer, several companies are already looking for alternatives to conventional plastics. Degradable polymers, such as polylactic acid, are therefore being used in a variety of applications, including housewares, food packaging, fabrics, and containers.

To ensure that they can perform their desired function but ultimately degrade at the end of their lifetime, it is essential to study the stability of degradable polymers under a wide range of conditions [12]. These conditions should include exposure to ultraviolet light, outdoor contact, heat aging, anaerobic biodegradation by specific microorganisms, aerobic or anaerobic biodegradation in the presence of municipal sewage sludge, aerobic biodegradation under controlled composting conditions or in aqueous media (e.g. seawater), and aerobic biodegradation in the marine environment by a defined microbial consortium among others [13]. Current characterization methods to study polymer degradation include simple techniques such as water uptake or macroscopic visual observation, since polymer degradation leads to cracks or changes in color [13]. For microscopic observation, methods like scanning electron microscopy (SEM) and atomic force microscopy (AFM) are used. Other techniques like Fourier transform infrared spectroscopy (FTIR), differential scanning calorimetry (DSC), nuclear magnetic resonance spectroscopy (NMR), differential thermal analysis (DTA), or X-ray photoelectron spectroscopy (XPS) are used to assess the biodegradability [13]. Gravimetric measurements, like thermogravimetric analysis (TGA) or quartz crystal microbalance (QCM), are also used. Other methods include enzyme assays, plate tests, respiration tests, and controlled composting tests [13]. However, the manner in which a polymer degrades depends not only on the degradation environment, but on the properties of the polymer itself, which can change

depending on the manner in which the polymer is processed. Polymer thin films, which have low overall starting mass, are particularly challenging to characterize.

In this thesis, I will describe one alternative: measurement of degradation using diffraction gratings. This is an in situ technique in which the first order diffraction spots generated by a grating on the surface of the polymer are tracked over time. In the specific case of tracking polymer thin film behavior, diffraction gratings can be used to evaluate the stability of polymer thin films under different degradation environments. In previous work, our group studied the stability of films of a highly crystalline thermoplastic biobased biopolymer: polyhydroxybutyrate (PHB). Our group proposed a diffraction-based method to evaluate PHB thin film stability in different conditions [14]. In that project, PHB films were immersed in degradation solutions with high and low concentrations of the enzyme *Comamonas testosteroni*. The resultant plots shows the changes in the diffracted beam intensity as time passed, which demonstrates that the beam intensity decreases as the grating diminishes in height. These results were corroborated by AFM and manual observations. These plots were compared with a control solution containing only the buffer, as shown in Figure 1.1.

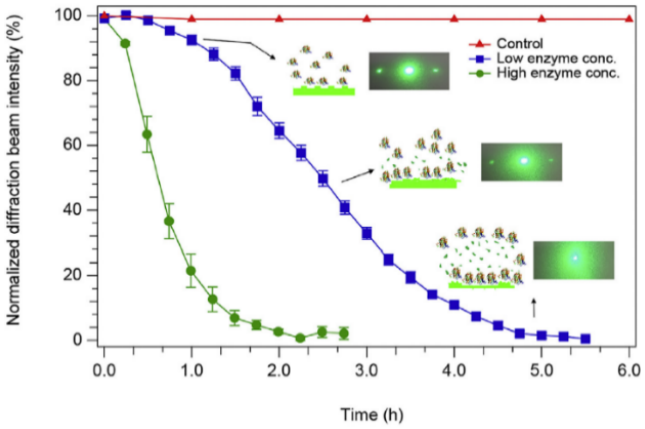

Figure 1.1. Diffraction results from PHB degradation evaluated with the diffraction-based method under none, low and high enzyme concentration. © 2017 P. Anbukarasu reproduce with permission [14]

From these plots, a probabilistic model was used to estimate an approximate mass loss and degradation rate. However, the model provided only qualitative data since it assumed a linear relationship between the supposed edge units of the grating and the diffraction intensity [14].

In this work, I propose to further develop the technique by rigorously simulating the output of diffraction gratings with various shapes and matching the diffracted intensity profiles with measured data. I also aim to ensure the method is more general by studying a different polymer: PLA.

I use PLA since it is one of the most widely used biodegradable polymers. To analyze the films with this approach, I modify the setup, the degradation conditions, and also utilize different diffraction grating shapes. I use the experimental results together with simulation software (OmniSim) to obtain quantitative data to study polymer thin film degradation. The use of this software is expected to provide theoretical information about the relationship between the change in the shape of the grating and the change in the diffraction intensity.

In this work, I will use my experimental data to calculate a PLA thin film etch rate under different degradation conditions. This important information should enable quantitative data of polymer thin films degradation. Knowing how the degradation rate is affected by various conditions will make it possible to better understand polymer thin film behavior. These results will help to select the right polymer for the right application based on the stability, dissolution and degradation of polymer thin films.

Objectives of the study

The objectives of this work are:

1. Track the behavior of PLA thin films under different degradation conditions with proteinase K as the enzyme
2. Based on simulations of diffraction gratings, develop a method to calculate the PLA etch rate from optical diffraction data
3. Evaluate the influence of different grating shapes on the degradation rate of PLA films

This thesis is divided into five chapters. Chapter 1 introduces the motivation of this work, while Chapter 2 provides a literature review of biopolymers, especially PLA, its degradation, and polymer thin films.

Chapter 3 describes the chemicals, materials, and experimental methods used to prepare the PLA thin films as well as the techniques used to characterize the materials. Additionally, the experimental setup used to evaluate PLA degradation is also described in detail. I also present the atomic force microscopy techniques used to characterize the various diffraction grating molds, intermediate PDMS molds, and PLA films, as well as to validate the results obtained by our diffraction-based optical characterization method. Additionally, I describe the OmniSim software that was used to calculate the PLA etch rates based on the experimental data.

Chapter 4 presents the characterization of the master molds, intermediate PDMS molds, and the PLA films prior to any degradation experiments. Subsequently, this chapter presents the results of the degradation experiments with two types of diffraction grating geometries: triangular and elliptical. The results of these different degradation experiments are used to obtain quantitative information using OmniSim simulation software.

Finally, the thesis concludes with Chapter 5, which summarizes the conclusions and future work from the existing project.

2. Background

This chapter presents an overview of terms and concepts relevant to the thesis work. It includes information about biopolymers, including polylactic acid (PLA), and the degradation mechanisms of PLA are also presented. Some PLA applications and polymer thin-film characterization methods are noted. Finally, the diffraction-based method for monitoring thin-film degradation is described.

2.1 Biopolymers

Polymeric materials have been present throughout human history. Since the first civilizations used rubbers, resins, and waxes, polymers have played significant roles in humans' daily lives through most of recorded history. Their use can be traced to ancient civilizations like Egyptians and Mayans [15]. Nevertheless, when the production of fuel-based polymers started last century, the overall scale of polymer usage dramatically increased. Nowadays, the extensive usage of plastic is unquestionable, and this use is due to the outstanding characteristics of polymers. Current conventional synthetic polymers like polyethylene (PE), polypropylene (PP), polystyrene (PS), poly(vinyl chloride) (PVC) and poly(ethylene terephthalate) (PET) are remarkably cheap to fabricate [6]. In 2015 alone, 448 million tons of polymers were produced [16] for use in construction, the automotive industry, industrial machinery, transportation, electrical insulation, textiles, medicine, consumer products, packaging and electronic apparatus [16]. However, degradation times for these polymers most readily available in the market extend to hundreds of years [6]. According to the United States Environmental Protection Agency, in the last 50 years, humans have produced more garbage than in the whole prior history of humanity [17]. This information concurs with the fact that nearly 50% of polymer production is only for packaging products [18]. These products are single-use polymers that are usually disposed of inadequately, contributing to the increasing amount of garbage in the land and the ocean [18]. The amount of discarded waste continues to increase [4]. Since the excessive production and consumption of oil-based polymers started in 1950, plastic waste production has become an increasing problem. This situation affects the environment and threatens to become a public health problem. For example, anthropogenic debris is already found in at least 25% of fish species designated for human consumption [19].

This plastic waste present in the ocean originates from several sources: ineffective removal mechanisms in plastic production, disposal of microbeads originally made for industrial manufacturing, microbeads for exfoliants in personal care products (which make their way through the plumbing system), fiber fragments from laundering synthetic fabrics, aqua-tourism residues, and broken fishing items, among others [10]. Since these materials cannot degrade in a timely manner, their physical size is slowly reduced by the effects of high salinity, microorganisms in the marine environment, UV-light exposure, and wave motion, generating microplastics that are already found in fish and sea birds [10], [16], [20]. The particle size of these plastics determines which sea animals will ingest it [10]. Depending on the marine species, this pollution can find its way back to human consumption.

Additionally, microplastics can also adsorb chemical and biological contaminants [20]. Studies about the consequences of microplastic consumption on humans remain unclear about these effects [19]. However, the ingestion of chemical additives is not generally favorable.

Different strategies have been proposed to diminish the excessive introduction of microplastics into the environment. For instance, changing from fossil fuel plastics to environmentally-friendly alternatives can reduce waste production [18]. Within these alternatives, some biopolymers are considered a potential “green” solution to the plastic waste problem due to their biodegradability [18].

Biopolymers (also called bioplastics) comprise both biodegradable polymers and bio-derived polymers [21] [22]. It is important to remark on the differences between the terms bio-plastic, biodegradable plastic and bio-based plastic since they can be easily confused. Bioplastics also include biodegradable polymers, i.e., polymers that can be degraded by microorganisms. This classification also includes biodegradable polymers even when they are petroleum-based such as polycaprolactone (PCL) or polybutylene succinate (PBS) [22]. Some biodegradable polymers are manufactured from fossil materials and some bio-based polymers are not biodegradable [22], [23]. Nevertheless, some biopolymers are both biodegradable and bio-based; therefore, they can help diminish the quantity of plastic waste and the consumption of fossil fuel resources [22]. To clarify this, Figure 2.1 demonstrates the intrinsic relationship between bioplastics, biodegradable plastics, and bio-based plastics [22].

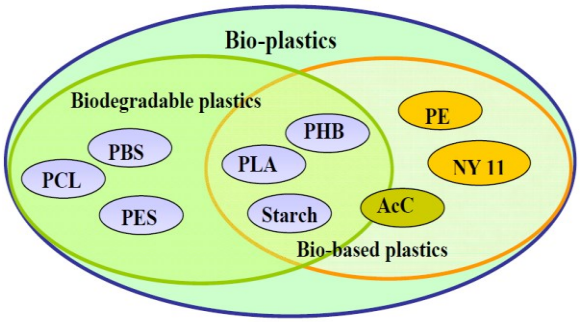

Figure 2.1. Bioplastics, which include both biodegradable and biobased plastics [22].

There exist different types of bioplastics; globally, they cover 300,000 metric tons of the plastic market, which only represents 1% of the 181 million metric tons of synthetic plastic production [24]. Bio-based polymers (such as polyhydroxybutyrate (PHB) and starch blends [25]) are produced by living microorganisms or made from renewable resources [26]. They are obtained from biomass feedstock that can be converted into raw materials used in polymer production, reducing fossil resource consumption [27]. On the other side, fossil-fuel polymers require millions of years to obtain their feedstock (i.e., petroleum) and hundreds of years to degrade [25].

Biodegradable polymers can be degraded by the action of microorganisms like bacteria, fungi, and algae [28]. Even though bio-degradation is generally benign, the majority of polymers available in the market are not biodegradable [8]. There are several types of biodegradable polymers, which can be classified into four main groups according to their source: (1) biomass, (2) microbial production, (3) chemically synthesized using monomers obtained from agro-resources and (4) polymers chemically synthesized from fossil fuel resources [18]. Table 2-1 shows this biodegradable polymer classification.

Table 2-1. Biodegradable polymers classification. © 2017 Moataz Elsay reproduced with permission [18].

No.	Category	Group	Example
1	Polymers from biomass	Polysaccharides	-Starches (wheat, potatoes, maize) -Cellulose and lingo-cellulose products (wood, straws, etc.) -Others (pectins, chitosan/chitin, gums)
		Protein and lipids	Animals (casein, whey, collagen/gelatin) Plants (zein, soya, gluten)
2	Polymers obtained via microbial production	Polyhydroxyalkanoates (PHA)	-Poly(hydroxybutyrate) (PHB) -Poly(hydroxybutyrate-cohydroxyvalerate) (PHBV)
3	Polymers chemically synthesized using monomers obtained from agro-resources	Poly(hydroxyacid) (PHA)	-Polyglycolic acid (PGA) -Poly(lactic acid) (PLA)
4	Polymers chemically synthesized from fossil fuel resources	Aliphatic co-polyesters	Poly(butykene adipate-co-terephtalate (PBSA)
		Aromatic co-polyesters	Poly(butylene succinate adipate) (PBAT)
		Others	Polycaprolactones (PCL), polyesteramides (PEA)

The biodegradation of polymers is affected by molecular weight which refers to the average molecular weight (in g/mol) of the constituent polymer chains, and it is intrinsically related to different physical properties like tensile strength, thermal behavior, toughness, and chemical resistance [29]. Other factors also influencing the biodegradability of polymers are the chemical structure, crystallinity, glass transition temperature (T_g), and processing of the material [24], [30]. Biodegradable polymers can be obtained by natural resources or synthetic resins [24]. Within the set of biodegradable polymers chemically synthesized from renewable resources exists polylactic acid (PLA), which is the key biopolymer of interest in this thesis.

2.1.1 Characterization methods for polymer degradation

To determine which polymer best suits a given application, it is necessary to study the properties of the polymer. Because plastic waste accumulation has become such a pressing issue, it has now become critical to understand the stability of polymers under different environments in addition to the more conventional thermo/mechanical characterization. Therefore, several techniques exist to study polymer degradation, including:

- Visual observation

It is possible to observe polymer degradation based on changes in the surface, such as the formation of holes and cracks. To obtain more information, several techniques like scanning electrone microscope (SEM), atomic force microscopy (AFM), or contact angle measurements can be utilized to know more about the degradation mechanism [13].

- Gravimetric techniques

Gravimetric techniques track the specimen mass before and after (or during) a specific process to study the mass loss in the degradation process [13]. These techniques are some of the most used methods to know residual materials and changes in polymer structure [13]. It is possible to obtain information about the degradation process by combining analysis of the residue with knowledge of the intermediates [13].

- Enzyme assays

In enzyme assays, the polymer is exposed to a medium containing purified enzymes [13], and these enzymes chemically attack the polymer according to their activity and environmental conditions. These assays are useful to study the release of degradation products, and it is possible to obtain quantitative information [13].

- Plate tests

Plate tests were developed to observe microbial degradation [13]. In these studies, the material is placed on an agar surface in a petri dish without any additional carbon source [13]. The petri dishes are then incubated at a constant temperature (approximately 21-28 days) with previously-selected bacteria or fungi [13]. From these studies, it is possible to know if the polymer substrate will resist the depolymerization caused by microorganisms [13].

- Respiration tests

Respiration tests are based on studying the production of CO_2 or O_2 in a controlled microbial environment [13]. In these tests, the polymer is placed in a degrading medium (e.g.

soil) and air sampling will be made to determine the amount of the byproducts [13]. Using the ratio of the biological oxygen demand (BOD) to the theoretical oxygen demand (TOD), it is possible to obtain information about the biodegradation process [13].

- Controlled composting tests

Compostability is one of the main advantages of biodegradable plastics [13]. For composting tests, the conditions may vary according to the complex and heterogeneous situations of the composts [13], but in general, the tests measure the composting rate for the test polymer. There are several regulations for different compost tests, which can include the percentage of humidity, the measured intervals and the quantity of the products in the remaining compost [13].

2.2 Polylactic acid (PLA)

Polylactic acid is derived from lactic acid (2-hydroxy propionic acid) [31]. It is a biocompatible, bio-based, and biodegradable thermoplastic aliphatic polyester usually derived by fermentation from natural resources [18]. It was discovered in 1845 by Théophile-Jules Pelouze, and in 1932, Wallace Hume Carothers et al. established a method to produce PLA in the laboratory[32]. Carothers' process, i.e., condensation of lactic acid, was patented by DuPont some years later [23], [32], [33]. PLA can also be synthesized by ring-opening polymerization of an intermediate called lactide and its chemical structure is shown in Figure 2.2 [34].

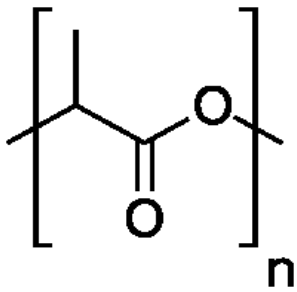

Figure 2.2. Chemical structure of polylactic acid [23].

Lactic acid is a chiral molecule with two stereoisomers, L- and D-lactic acid [35]. Depending on the ratio of these enantiomers along the polymer chain, PLA can be present in three stereochemical forms, poly(L-lactide) (PLLA), poly(D-lactide) (PDLA), and the racemic mixture of both, called poly(DL-lactide) (PDLLA) [22]. PLA properties can vary according to their stereochemical structure and enantiomer ratios [36], primarily through variations in

crystallinity [37], [35]. It is possible to obtain control over the resulting properties of PLA since the proportions of the isomeric acid units can be altered [35]. Depending on the type of PLA, its optical, mechanical, thermal and barrier properties can be comparable to those of commodity polymers like polypropylene (PP), polystyrene (PS) and polyethylene terephthalate (PET) [25]. Some properties of different PLAs are mentioned in Table 2-2.

Table 2-2. General properties of different PLAs. © Farah, reproduced with permission [38].

Properties[a]	**Type of biopolymer**			
	Unit	PLA	PLLA	PDLLA
$\boldsymbol{\rho}$	g/cm^3	1.21-1.25	1.24-1.30	1.25-1.27
$\boldsymbol{\sigma}$	MPa	21-60	15.5-150	27.6-50
$\boldsymbol{E}$	GPa	0.35-3.5	2.7-4.14	1-3.45
$\boldsymbol{\varepsilon}$	%	2.5-6	3.0-10.0	2.0-10.0
$\boldsymbol{\sigma^*}$	Nm/g	16.8-48.0	40.0-66.8	22.1-39.4
$\boldsymbol{E^*}$	kNm/g	0.28-2.80	2.23-3.85	0.80-2.36
$\boldsymbol{T_g}$	^{o}C	45-60	55-65	50-60
$\boldsymbol{T_m}$	^{o}C	150-162	170-200	am[b]

[a] ρ— Polymer density, σ — tensile strength, E — tensile modulus, ε — ultimate strain, σ* — specific tensile strength, E*— specific tensile modulus, Tg — glass transition temperature and Tm — melting temperature. [b] am — amorphous and thus no melt point.

One of the main advantages of PLA is its biodegradability. This polymer is environmentally-friendly during its life cycle, as can be observed in Figure 2.3.

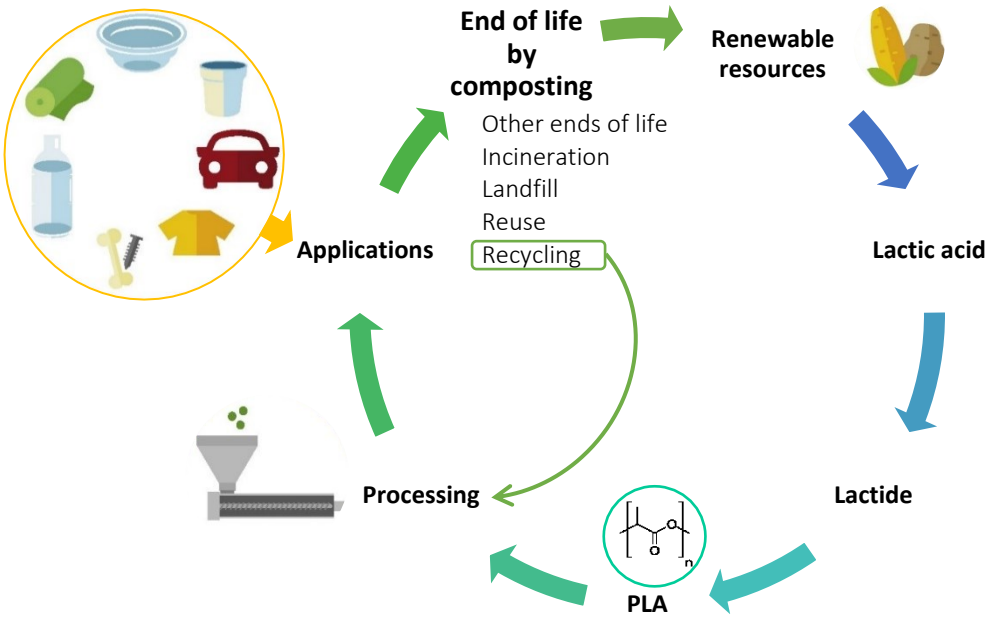

Figure 2.3. Polylactic acid derived from renewable resources such as corn starch can be processed to obtain different products, and by recycling or composting can return to the processing stage or the beginning, respectively. © 2016 E. Castro Aguirre reproduced with permission [25].

Being one of the most used bio-based polymers, PLA can help reduce the dependence on petroleum-based materials by replacing a fraction of these fuel-based polymers [24], [38]

2.2.1 PLA degradation mechanisms

The study of PLA biodegradability and biodegradation mechanisms provides a better understanding of its service-life [39]. PLA biodegradation is a process where the chemical structure undergoes significant changes that result in the loss of properties [25]. These changes involve bond scission in the backbone under specific environmental conditions as driven by chemical, biological and physical forces [9]. When PLA degrades, it undergoes a decrease in molecular weight (M_w) and an increase in M_w distribution [25]. Different factors influence the degradation process like structure, morphology, additives, environmental conditions, stereoisomeric content, crystallinity and initial molecular weight [13].

PLA degradation can be abiotic or biotic, and within these types of degradation, there are different mechanisms, as shown in Figure 2.4.

.

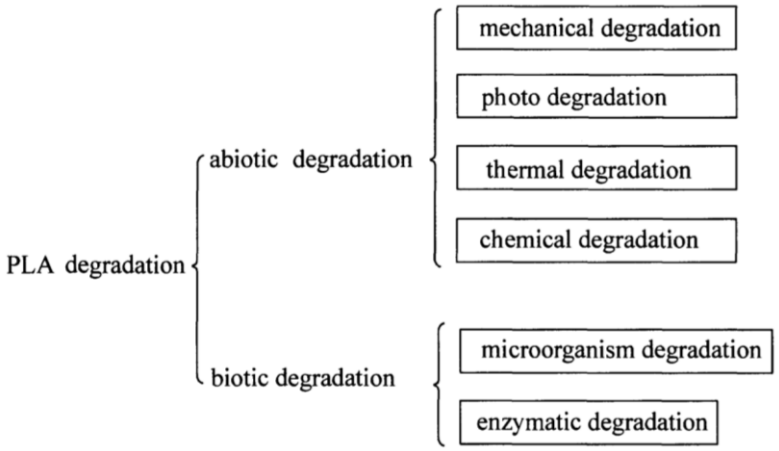

Figure 2.4. PLA degradation mechanisms. © 2010 J. Ren reproduced with permission [13].

The abiotic mechanisms are mechanical degradation, photodegradation, thermal degradation, and chemical degradation, each of which will be discussed below [25].

Mechanical degradation

Mechanical degradation involves the application of forces to break the plastics physically. These forces can be compression, tension or shear forces [13]. Even when this type of degradation is not the main factor, mechanically-induced damage can start or accelerate the biodegradation by increasing surface area [13].

Photodegradation

PLA can be susceptible to sun exposure. The UV radiation causes photodegradation due to the high-energy, short-wavelength UV radiation [25]. This radiation breaks chemical bonds in the polymer, which drives changes in polymer properties due to the reduction in M_w [25].

Some biomedical products require UV irradiation for sterilization, and PLA can suffer different effects as a consequence of UV irradiation. These changes in molecular weight cause PLA to become brittle over time due to the heterogeneity of the structure [25]. Additionally, an increase in UV exposure causes faster degradation [25]. Other types of irradiation, such as γ-irradiation, may also affect PLA [25].

Thermal degradation

PLA can be thermally degraded when it is processed at high temperatures [40]. This type of degradation leads to a decrease in rheological and mechanical properties [25]. Thermal degradation of PLA is due to diverse factors, including random main-chain scission reactions, depolymerization, and oxidative degradation [12]. These processes are driven by thermal energy

which promotes the oxidation of carbon in the polymer backbone [13]. Additionally, several different parameters potentially enhance the thermal decomposition of PLA, such as active chain-end groups, residual catalysts, residual monomers, and other impurities [40]. Thermal degradation is a complex chemical mechanism that can be related to other mechanisms such as hydrolysis (when moisture is present) [25], [40], [41].

Chemical degradation

As a polyester, PLA is particularly attractive among biodegradable plastics because of its potentially hydrolyzable ester bonds [24]. PLA is synthesized by condensation, and these polymers are sensitive to degradation by hydrolysis [42].

Hydrolytic degradation occurs in the presence of moisture, and the diffusion of water into the polymer bulk limits the rate of hydrolysis [42]. First, water needs to be absorbed on the surface to permeate into subsurface regions [47]. The cleavage of ester groups along the main chain and the release of soluble oligomers and monomers causes a decrease in molecular weight [25]. Another factor that influences hydrolytic instability is the flexibility of polymer chains, as more flexible chains are more open to moisture penetration [42]. Hydrolysis is considered to mainly occur in amorphous regions due to the lack of structure in these regions, which facilitates the penetration of water molecules [42]. After the cleavage has started, the degradation continues in the boundary layer of the crystalline areas [25].

Polylactic acid is a polyester. Figure 2.5 shows its alkaline catalyzed hydrolysis. Ester bonds are hydrolyzed by the nucleophilic substitution by addition-elimination mechanism. The first part consists on the addition of the nucleophile (water). Subsequently, it occurs the elimination of a leaving group since the tetrahedral intermediate is high in energy to expel it. Then, the carboxylic acid is too basic to survive. Therefore, a carboxylate anion and an end group are created.

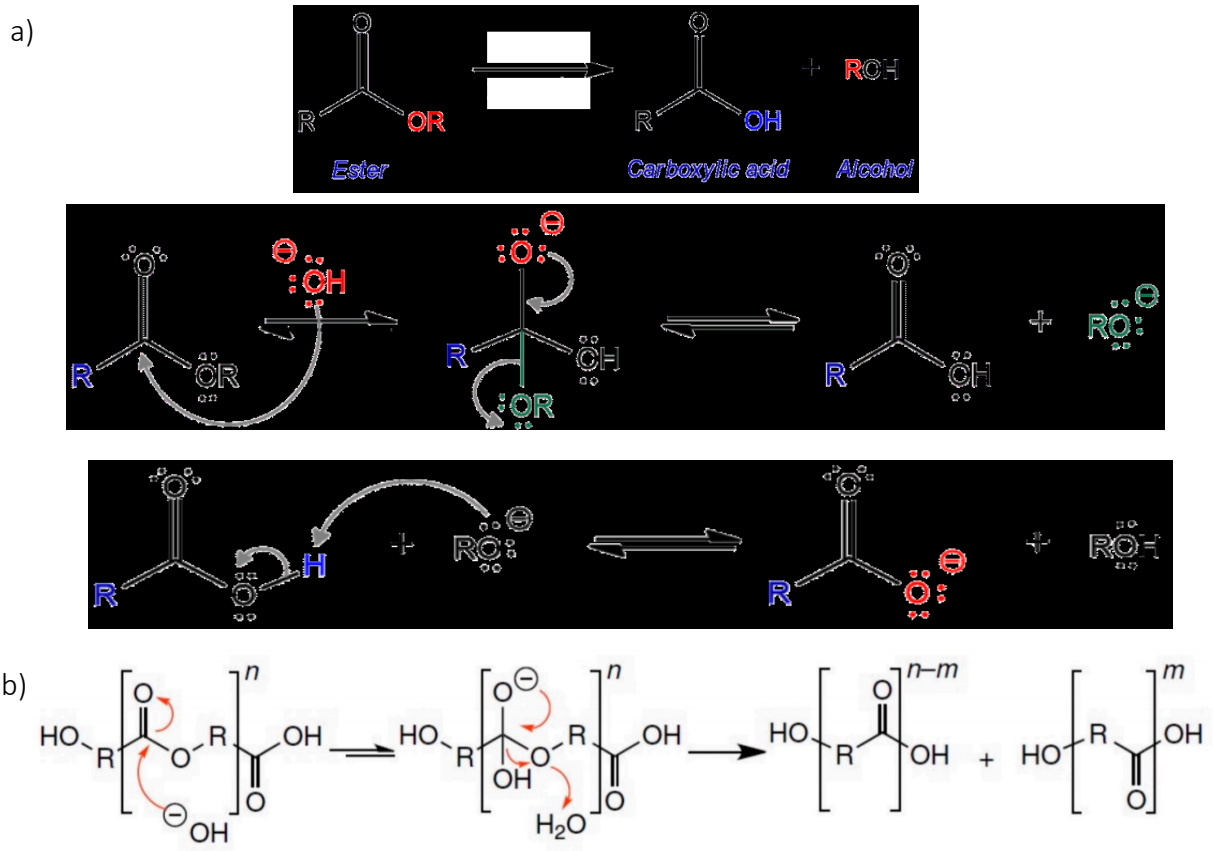

Figure 2.5. Alkaline-catalysed hydrolysis for a) ester and for b) polyester hydrolysis [43].

The biotic degradation mechanisms include enzymatic degradation and microorganism degradation [25], each of which is discussed below. In general, PLA possesses hydrolysable ester bonds, and these bonds are chemically attacked by bio-derived species [44].

Enzymatic degradation of PLA

One manner by which microorganisms degrade PLA is by excreting enzymes, causing a catalyzed hydrolytic degradation [45]. Enzymes such as proteinase K from *Tritirachium album* [45], lipase from *Candida cylindracea* [46], esterase from porcine livers [47], and alcalase from *Bacillus lichenifromis* [46] can degrade this polymer. However, the majority of the literature focuses on PLA degradation by proteinase K [48].

The first report on the degradation of PLA under the action of proteinase K was made by Williams in 1981 [45]. Since Williams first demonstrated that proteinase K could degrade PLA, this enzyme has been used for studying the degradation characteristics of PLA, PLA blends, and copolymers of PLA [49], [50]. The enzymatic degradation of PLA by hydrolysis is a two-step process [22], [49]. First, the enzyme is adsorbed on the surface through the surface-

binding domain causing surface erosion [51]. Then, the enzyme penetrates further into the interior, hydrolyzing ester bonds, as shown in Figure 2.6 [49] There exist some intermediate products that are dissolved into the medium [51]. These intermediate products can be low molecular weight oligomers, dimers, and monomers that can be mineralized into end products like CO_2 and H_2O [22].

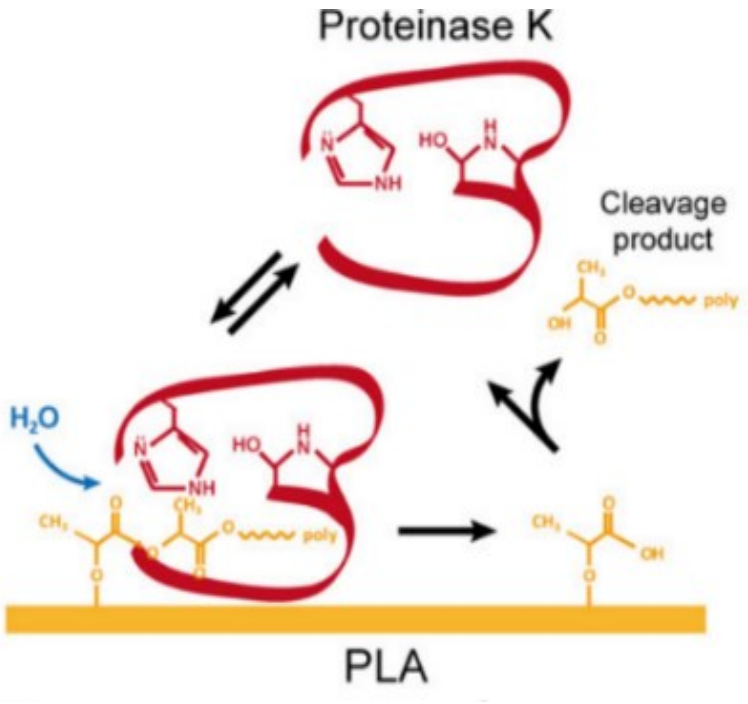

Figure 2.6. PLA enzymatic degradation by proteinase K. © 2010 Victor Ugaz used with permission [52].

Degradation studies suggest that enzymatic hydrolysis is faster in amorphous regions than in crystalline regions since water diffusion can be restricted within crystalline structures [34]. This preference increases the crystallinity of the polymer during degradation and decreases the degradation rate over time [49].

Enzymes work as biological catalysts, and enzyme activity is a measure of the quantity of active enzyme; therefore, it is a measure of the catalytic ability [53]. Different factors affect enzyme activity, including, enzyme concentration, substrate concentration, inhibitors, temperature, and pH [54]. The active enzyme concentration can be limited by the availability of the substrate to which it can bind. The enzyme activity is affected by changes in pH, as shown in Figure 2.7 (a). The highest point is known as the optimum pH, where the enzyme is most active, obtaining a maximum reaction velocity. Temperature effects are shown in Figure 2.7

(b). For the majority of chemical reactions, an increase in temperature generally leads to a rise of enzyme-catalyzed reactions [54]. However, most enzymes are adversely affected by high temperatures [53]. Therefore, activity drops off once a specific temperature is exceeded. Also, it is necessary to consider that over some time, enzymes will lose their activity even at lower temperatures.

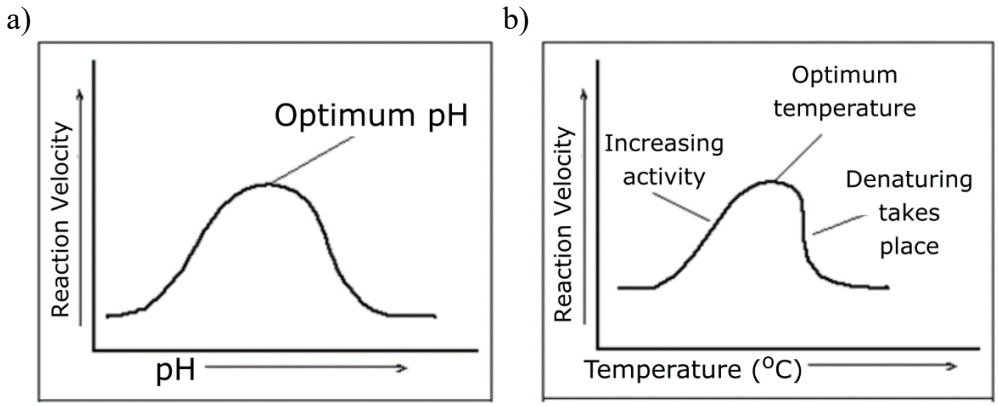

Figure 2.7. Effect of a) pH and b) temperature in enzyme activity. © 2007 Worthington Biochemical Corp. reproduced with permission [54]

Microorganism degradation

Microorganism degradation includes biodegradation caused by bacteria, fungi, and algae. The general mechanism of this type of degradation is presented in Figure 2.8.

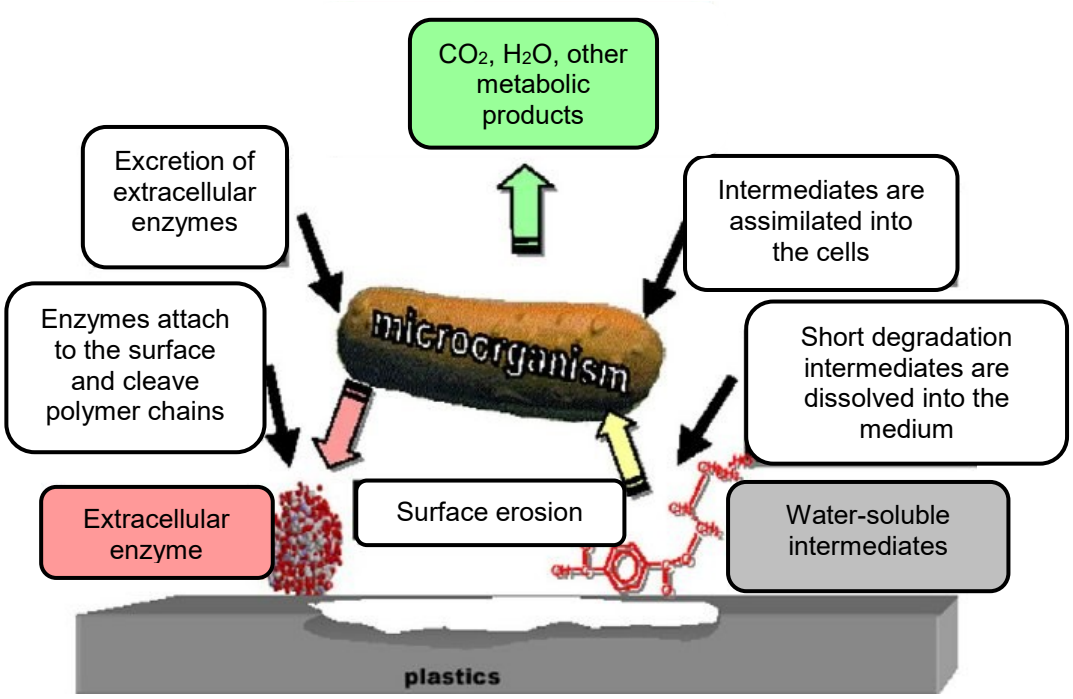

Figure 2.8. Mechanism of microorganism degradation of plastics. ©2006 Rolf-Joachim Mueller reproduced with permission [55]

Despite numerous studies about PLA biodegradation, conditions that effectively catalyze the degradation of this material in different soil or marine environments have not been found. Other synthetic aliphatic polyesters like polyhydroxybutyrate (PHB), polycaprolactone (PCL), and polybutylene succinate (PBS) are more sensitive to microbial attacks due to the microorganisms present in the environment [49]. PLA degradation studies have been focused on enzymatic degradation. However, PLA can also be degraded by the action of different microorganisms [49]. Microbial degradation of PLA has been studied with *Amycolatopsis* strain since 1997 [56]. PLLA has been the primary PLA studied since it presents desired properties such as a high degree of transparency, ease of fabrication, and high melting point [34]. Therefore, several studies have been made with different isolated strains like *Lentzea, Kibdelosporangium, Streptoalloteichus,* and *Saccharothrix* that were able to degrade PLLA [49].

2.2.2 PLA applications

The first applications of PLA were in biomedicine in the early 1960s [25]. PLA biocompatibility caused this extensive use since it degrades into its harmless monomer, lactic acid [18]. The body normally produces lactic acid, and it has not shown any toxicity in humans [25]. Its biomedical applications include drug delivery systems, delivery and protein

encapsulation, controlled-release devices, microspheres, hydrogels, resorbable sutures, implants for orthopedic surgery used for internal bone fracture fixation and bone reconstruction [18] [57] [58].

Until the late 1980s, PLA was restricted to medical applications due to low availability and high production costs, and limited molecular weight (M_w) [59].[25]. Initially, PLA was synthesized by ring-opening polymerization resulting in low molecular weight PLA [43], [60]. However, through a low-cost process like direct polycondensation of lactic acid, it is now possible to obtain high molecular weight PLA [59], [60]. Thanks to these advances the PLA properties are sufficient for different applications [25]. PLA possesses remarkable characteristics such as its biocompatibility, low toxicity, good appearance, high mechanical strength, outstanding barrier properties, stiffness, and thermo-plasticity [61]. Due to its properties, this polymer has several applications in various fields other than medicine. Nowadays, PLA applications include containers, fabrics, building materials, transportation, agriculture, electrical appliances, food packaging, electronics, and housewares [25], [61]. To make the variety of applications possible, PLA is manufactured by different processes like injection molding, blow molding, foaming, fiber spinning, melt spinning, thermoforming, as well as sheet and cast film extrusion [25].

PLA applications are as broad as their different formats. PLA can be present as pellets, extruded filaments, fibers, and polymer thin films. Additionally, the PLA permeability performance against the transfer of aromatic molecules, water vapor, and gases is remarkable [61]. PLA has been proposed to be used in thin films since, in this application, plastics are hard to recover through recycling [25]. PLA films are an attractive plastic in the manufacture of disposable items like wraps, food packaging, or deli trays.

2.2.3 Polymer thin films

Polymer thin films are used as functional and protective coatings, antifriction layers, in optoelectronics, bioelectronics components, microelectronic devices, food packaging, sensors, radiation detectors, tissue engineering, wound healing materials, compostable bags and environmental remediation films [25] [14] [62].

However, polymer thin films are difficult to recycle due to their tendency to obstruct the recycling machinery (e.g., plastic bags clogging rotating axles). Additionally, polymer thin films can be too contaminated to recycle after fulfilling one of their primary functions (e.g.

containing and transporting food waste or medical residues) [63]. Regarding the other applications of polymer thin films, their recovery can be hard due to their dimensions.

Another alternative to avoid the disposal of these films is to degrade them. Even though polymer thin films have so many different applications, characterizing their degradation remains a challenge, and there are still many questions about the interactions between polymer thin films and their environments. It is of great importance to understand the influence of the degradation environment on the degradation because, for some uses, polymer thin films require high stability, while for others, they may need to show a faster degradation rate [64]. For instance, polymer thin films used in microelectronics require high stability, while for tissue engineering or sensors, they need to degrade in a shorter period under very specific conditions [65], [66].

The manner in which a polymer degrades not only depends on the degradation environment, but on the properties of the polymer itself, which can change depending on the manner in which the polymer is processed. Polymer thin films, which have low overall starting mass, are particularly challenging to characterize.

There exist specific properties associated with biodegradability like first-order properties (molecular weight distribution and chemical structure), high order properties (crystallinity, glass transition temperature, melting temperature and elastic modulus), and surface conditions (surface area, hydrophilic and hydrophobic properties) [22]. In polymer thin films, surface free energy, and high surface to volume ratio become dominant factors (especially as compared with bulk materials) [67]. Due to these differences, polymer thin films and the bulk polymer can behave differently under the same degradation conditions [14]. It is highly relevant to understand the stability and degradation of polymer thin films; however, current characterization techniques tend to be focused on bulk materials [14].

2.2.4 Characterization methods for polymer thin films

Most existing methods to characterize bulk materials are focused on gravimetric techniques; however, they are often unable to track small-scale mass loss changes within thin films. For this reason, polymer thin film characterization is difficult due to the high sensitivity required. Some current methods that attempt to cover this issue are advanced gravimetric techniques like resonant micro-cantilevers and quartz crystal microbalance (QCM) [14], [68]. Nevertheless, these methods need an exhaustive sample preparation and high precision equipment [69].

Fourier transform infrared spectroscopy (FT-IR) can obtain chemical and structural information [70]. This non-destructive method can observe oxidation, crystallization or cross-linking processes by monitoring specific functional groups [70]. However, FT-IR is constrained by the incident radiation wavelength-limited resolution [71].

Evanescent waveguide spectroscopy (WS) can also be used to measure the refractive indices of polymer thin film and the thickness [70]. This technique provides information when the films are deposited on a noble metal surface, thus, limiting its application to a specific case of polymer thin films [70]. In the case of very thin layers of polymers, an alternative is surface plasmon resonance (SPR), an optical technique that can also monitor the dissolution of polymer films [65], [70].

Additionally, gel permeation chromatography (GPC) also provides information about the degradation kinetics. This characterization technique is a high-performance liquid chromatography which uses precise specifications such as the use of helium, high-pressure pumps, columns and detectors. All these conditions imply a scrutinous and challenging process to obtain information from the sample [72].

For this reason, in this work, we proposed the use of a degradation sensor based on diffraction gratings used previously to characterize polymer thin films [14], [73]. This diffraction-based characterization method monitors the polymer thin film stability under an enzymatic degradation providing quantitative mass changes. Using this information, it would be possible to compare the behavior of PLA thin films under different degradation environments.

2.3 Diffraction gratings

Diffraction occurs when light deviates from rectilinear propagation when there is an obstruction [74]. Diffraction gratings are periodic arrays of diffracting elements (apertures or obstacles) that alter the amplitude and phase of an incident wave [74]. A common arrangement consists of a multiple-slit configuration or several thousand parallel grooves [74].

David Rittenhouse made the first diffraction grating in 1785, constructing a half-inch wide grating with fifty-three apertures. Years later, in 1821, Joseph von Fraunhofer deduced the equations of the dispersive behavior of gratings [75]. In the late 1800s, Robert and Rutherford started to fabricate gratings, however, it was not until 1900 that Rowland accentuated the

importance of the gratings, establishing it as the primary optical element in spectroscopy [75]. Subsequently, in 1950, Bausch & Lomb started to produce high-quality precision gratings [75].

When light is incident on a grating surface, it is diffracted from the grooves [75]. Each groove becomes a minimal source of reflected or transmitted light. Figure 2.9 shows how a reflection grating diffracts incident light of wavelength λ on the same side of the grating normal [75]. This grating has a groove spacing *d*, also known as *pitch* [75].

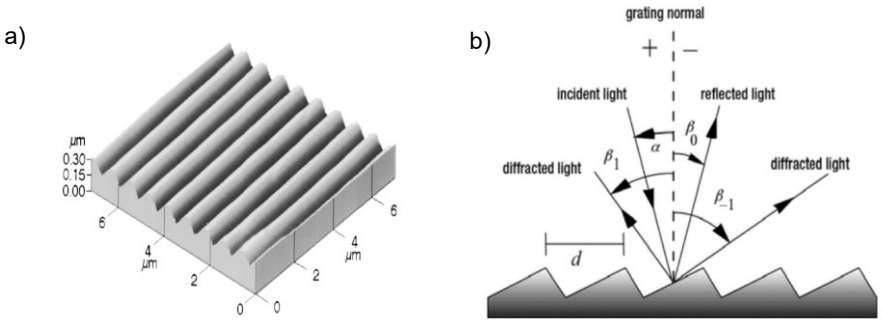

Figure 2.9. a) A diffraction grating and [75] b) schematic representation of the working principle of a diffraction grating. © 2005, Christopher Palmer, Newport corporation with permission [76].

The main characteristic of a grating is that there is a set of angles where the light scattered from all facets is in phase [75]. The angle of the output beam is given by the grating equation 1 [75].

$$d(\sin\theta_i \pm \sin\theta_m) = m\lambda, \qquad m = 0, \pm 1, \pm 2 \ldots \tag{1}$$

Where λ is the wavelength, θ_i is the angle of incidence, θ_m is the angle where the intensity maximum of that wavelength is found, and d is the grating period [75]. The grating period is usually measured in μm; however, its inverse called "groove" is given in grooves per mm (gr/mm) [75]. The term m indicates the diffracted beam order and $m = 1$ is usually preferred since it is generally the highest intensity order. The grating equation does not mention how much light goes in a specific direction, only the direction itself. The physical quantity that describes the distribution of the incident field power is the diffraction efficiency. In diffraction gratings, it is possible to vary the angle of diffraction by changing the distance and form of the grooves. Figure 2.10 shows the theoretical profile of a ruled blazed grating [77]. This type of grating with a "sawtooth profile" is also known as a blazed grating, and they exhibit, for specific orders and wavelengths, high diffraction efficiency minimizing power lost to other orders [78].

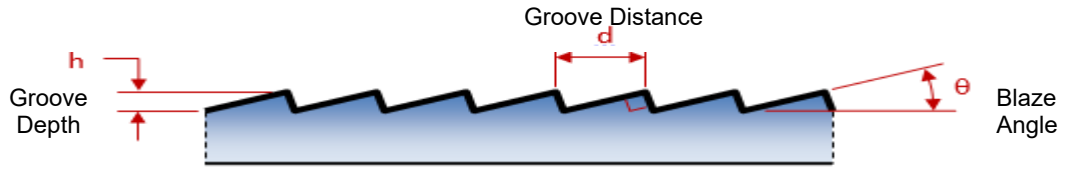

Figure 2.10. Groove characteristics for a diffraction grating. ©2020 Dynasil Corporation reproduced with permission [77].

The grooves can also have different shapes. They can be rectangular, trapezoidal, triangular, and sinusoidal [75]. Figure 2.11 shows various possible forms for a diffraction grating.

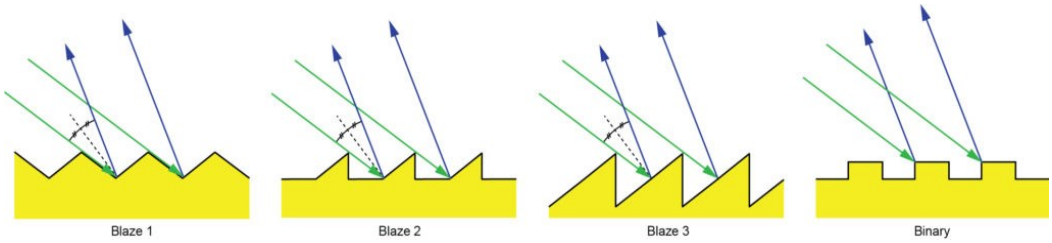

Figure 2.11. Different blaze angles and groove shapes of diffraction gratings. © Turan Erdogan, used with permission from Plymouth Grating Laboratory, Diffraction Efficiency [79].

Each shape presents different characteristics. For example, rectangular gratings are used in the soft X-ray region, while sinusoidal grooves offer high diffraction efficiency at a broad range of wavelengths (which is determined by the groove depth) [78].

A diffraction grating is comprised of different layers: a substrate, a resin layer, and, in case of a holographic grating, a reflective coating [76]. The resin holds the groove pattern, a groove profile, the substrate keeps the surface rigid and the coating provides the reflectivity required for holographic gratings. Diffractive optical elements like diffraction gratings can be fabricated by lithographic methods, direct machining, and replication [80]. These techniques use several steps to create microstructures, which can promote the introduction of several variations [80]. One alternative to improve their performance is the method of direct machining, and this is a promising technique that refers to the direct removal of the material by different techniques [80]. These methods include mechanical ruling, focused ion beam milling, and diamond turning [80]. However, the high quality often comes at the expense of fabrication time [80]. Due to the time and costs needed to produce diffraction gratings by lithography and direct machining, it is desirable to use a "master" element to make reliable copies in other materials [80]. To obtain these reproductions, the preferred method used is replication [80]. This method

starts by forming the "master"; from this master, a diffraction grating can be obtained. Different replica methods are plastic injection molding, thermal embossing, and casting, each of which is shown in Figure 2.12 [80].

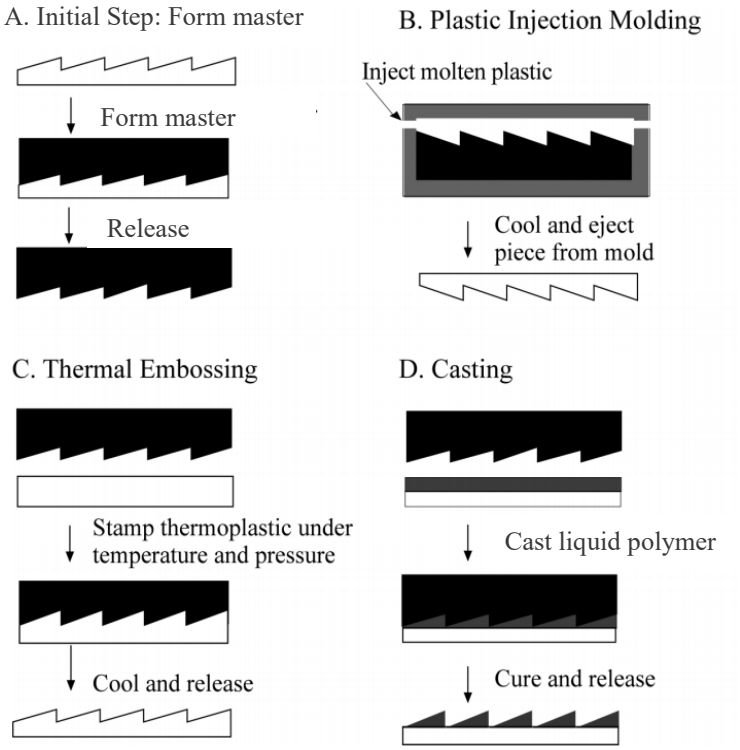

Figure 2.12. Replication process of diffraction gratings by three different techniques after forming the master. © 2003 Donald O'Shea reproduced with permission [80].

These methods are regularly used in modern society to produce volume manufacturing of diffraction gratings [80]. As the masters themselves may be delicate, intermediate molds can be fabricated for subsequent production of gratings. These molds should be made of a flexible material able to reproduce the same characteristics, and that can be used repeatedly, keeping the reproducibility of the features. At the same time, it is also necessary to consider the chemical affinity between surfaces and ensure that the "peeling off" or separation process can be performed without destroying either the intermediate or the replica.

2.3.1 Applications of diffraction gratings

Diffraction gratings have found numerous applications in different fields. Diffraction gratings have been used as monochromators to separate wavelengths of incident light in analytical laboratory instruments, such as spectrophotometry, Raman spectroscopy, and atomic

absorption [79]. Other applications include fiber-optic telecommunications networks, different laser devices, reflectance, beam splitters, and fluorescence [75] [76]. Regarding metrological applications, diffraction gratings can be employed to calibrate apparatus like atomic force microscopes (AFMs) and systems intended to measure strain and displacement [75].

Diffraction gratings can also be used in biosensing [81]. Diffraction-grating based sensors, fabricated of analyte-sensitive materials, have been used as qualitative diagnostic tools in the detection of clinical biomarkers [82], [83]. These optical-diffraction-based biosensors use the changes in diffraction signal intensity or the appearance of a diffraction pattern as signals of surface reactions [84]–[86]. These sensors offer a fast, highly selective, and high sensitivity response based on the diffraction phenomenon [83], [87].

Among the distinct applications of diffraction gratings, there is their use in biosensors using surface Plasmon resonance (SPR) and resonant waveguide grating (RWG), mainly used to determine affinities and kinetics [88]. Additionally, these sensors have been applied in sensing biomolecules, volatile organic compounds, DNA, and metal ions [83], [89]. These applications are appropriate because diffraction-grating sensors offer advantages like easy operation, broad applicability, and low cost [83]. This type of sensor uses specific responsive materials, able to provide a particular response to certain stimuli, arranged into periodic structures [90]. Depending on the analyte of interest, the arrays are designed to be influenced by different phenomena. The gratings can be modified by water displacement or by the interactions with target molecules resulting in changes in color or modifying the geometry of the periodic structure [85], [89]. The geometry of the gratings (grating period, groove depth, and aspect ratio) significantly influences the diffraction properties [91]. Hence, the variations from the geometrical parameters result in measurable optical signs [85]. These optical characteristics depend on their structure. However, there are no simple equations that connect intensity with grating shape. Consequently, simulation models have been considered the preferred methods to design and optimize these structures.

2.3.2 Simulations

The development of complex structured optical materials such as photonic crystals and metamaterials has driven a need for useful simulations [81]. Since the increasing amount of this type of material, the need to obtain more information from them has increased. Materials like metamaterials, plasmonic materials, and diffraction gratings possess specific characteristics that

cannot be replicated by other means. Additionally, their properties are determined by their physicochemical structures; therefore, it is essential to study the effect of structure on optical properties before fabrication to ensure the best application and performance. In the case of diffraction gratings, the grating equation provides information about where the light is directed [75], however, it cannot determine the relative power directed in each diffracted order [80]. The characteristics of the surface profile dictate the power distribution, and the grating period would define it by its nature and shape [80].

To be able to predict this information, in the last years, different simulation packages have been used. For instance, OmniSim software is a flexible program that can provide information about the grating efficiency, simulating the propagation of light through any design, and it includes an extensive material database [92]. This software can predict diffraction with reasonable accuracy. It considers only a single period of the grating, and you can introduce the fixed refractive index, the height, pitch, diffraction order, wavelength, and attenuation of the media [92].

2.4 Diffraction-based sensors

In previous work, our group introduced a diffraction-based sensor to evaluate the stability of polyhydroxybutyrate (PHB) thin films. PHB is a natural source thermoplastic produced by bacterial fermentation [93]. This highly crystalline thermoplastic, exhibiting biocompatibility and biodegradability, is applied in food packaging and drug delivery [94]. The proposed method was focused on the study of the stability of PHB thin films in the presence of *Comamonas testosteroni* [14]. This method measured the behavior of patterned PHB films under different enzyme concentrations.

The setup presents three main components comprised of a laser source, the polymer sample mounted in a plastic cuvette with the enzymatic solution, and the sensors measuring the first-order diffracted beam [14]. In this first publication describing this technique, the method focused on the evaluation of PHB stability under three conditions: no enzyme, low enzyme concentration, and high enzyme concentration [14]. From the experimental degradation data, a probabilistic model was proposed to estimate the degradation rate and a mass loss [14]. However, rather than considering the evolving shape of the diffraction grating, this model assumes that every atom of the grating structure contributes equivalently to the diffracted

output, and it did not provide a quantitative approximation of mass loss [14]. This model neither considers the effect of different shapes on the changes of the diffraction intensity. Furthermore, this analysis was done with PHB, a biopolymer with high crystallinity that results in an inhomogeneous degradation [14].

In a second work by my group, this method was used to study the effect of dimensional constraints in PHB films. These films possessed different thicknesses and were immersed in enzymatic solutions to evaluate the relationship between thickness, crystallinity and degradation rate [73]. These results are presented in Figure 2.13. However, this study still utilized with qualitative information and a general model able to provide quantitative information would contribute to further understanding of polymer degradation.

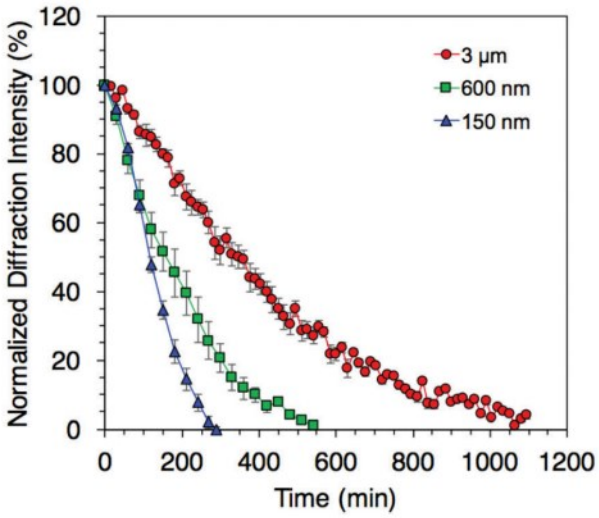

Figure 2.13. Normalized intensity versus time plot obtained from the diffraction-based method for PHB thin films of different thicknesses exposed to a $PhaZ_{cte}$ enzyme solution [73].

3. Experimental Methods

3.1 Materials

The polylactic acid (PLA, 4042D, Filabot, Saint Barre, VT, USA) used in this work was obtained as thermally processed pellets (98%), and it was washed with isopropyl alcohol (70%, Sigma Aldrich, Canada) before use in order to remove potential surface impurities. Dimethylformamide (98%), trizma hydrochloride (tris-HCl, 99%), glycerol (99%), calcium chloride (93%), hydrochloric acid (98%), sodium hydroxide (97%) and (1,1,2,2 H perfluorooctyl)-trichlorosilane (PFTS, 97%) were acquired from Sigma-Aldrich and used as received. Proteinase K from *Tritirachium album* was purchased from Sigma Aldrich as lyophilized powder. Polydimethylsiloxane (Sylgard 184 Silicone Elastomer Kit) was purchased from Dow Corning (Midland, Michigan, USA).

3.2 Mold preparation

Different mold geometries were used to produce different gratings. The triangular master mold (TMM, 1.6 μm periodicity, 650 nm step height) was purchased from Edmund Optics (Part #49580, New Jersey, USA). This mold is comprised of a polymer coating on top of a B270 glass substrate.

Elliptical grating master molds were fabricated by laser interference lithography by collaborators at the Leibniz Institute of Polymer Research in Dresden, Germany. The method is briefly summarized here. The beam of a He-Cd laser (Kimmon IK5351R-D, Tokyo, Japan) operating with a 325 nm emission wavelength was spatially filtered to achieve a well-defined Gaussian beam profile. The beam was then split into two separate paths (50:50 intensity ratio) with a non-polarizing fused silica plate beamsplitter (BSW20, Thorlabs Inc., New Jersey, USA). The two paths were then recombined at an angle of 9.4°, which resulted in an interference pattern with approximately 1 μm periodicity. This interference pattern was then recorded in a commercially-available SU-8 photoresist (microresist GmbH) on a silicon substrate with exposure doses varying from 2.6 mJ/cm² to 5.2 mJ/cm². Following this, the substrates were post-baked at 95°C for 60 s and developed for 30 s using mr-Dev600 (microresist GmbH). The gratings were then rinsed with ultrapure water (Merck Millipore) and dried under a nitrogen

flow. Master molds with groove heights of 110, 200, 212, 287, 356 and 470 nm were produced, and hereinafter referred to as E1, E2, E3, E4, E5 and E6, respectively.

The surfaces of the master molds were found to be highly delicate and susceptible to solvents. In order to avoid damage and extend the lifetime of the master molds, transition molds made with polydimethylsiloxane (PDMS) were required, and the process used to fabricate these intermediates is shown in Figure 3.1. PDMS was formed by thoroughly mixing the silicone elastomer base and the curing agent in a 10:1 volume ratio, stirring by hand for approximately 10 minutes, and degassing under low vacuum for 1 hour prior to casting. Following mixing and degassing, approximately 3 mL of PDMS was poured onto the surface of the triangular molds. The PDMS curing process was accelerated by heating for 15 min at 130°C in an oven. For the elliptical molds, the master mold with PDMS on top was degassed again for an additional 1h to remove trapped air bubbles and to enhance the geometry replication. After curing, the PDMS layer on the mold surface was carefully peeled off from the masters.

During PDMS casting, the silicon substrate from the elliptical SU-8 master molds is exposed to PDMS in some locations, and it presents a hydrophobic behavior with a high affinity to PDMS. For this reason, the SU-8 elliptical molds required a fluorosilane release layer before polydimethylsiloxane (PDMS) application to avoid any surface damage when the master and PDMS intermediate were separated [95]. The method used in this work was vapor-phase silanization. To protect their geometry, these SU-8 masters were placed in a 6 L vacuum desiccator with 2 drops (roughly 100 µL) of the (1,1,2,2 H perfluorooctyl)-trichlorosilane (PFTS, 97%) for 8h. The PDMS process was then performed as noted above.

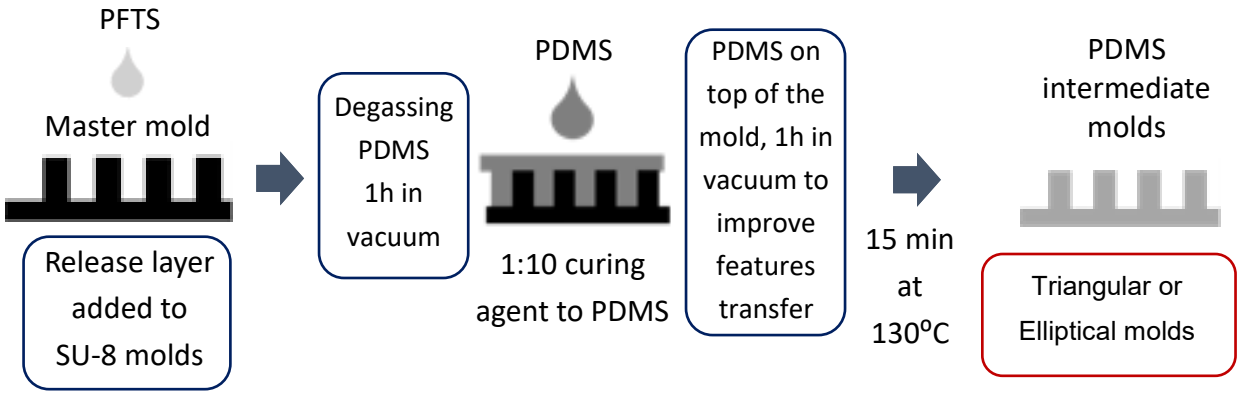

Figure 3.1. Replica process used to obtain PDMS intermediate molds (triangular and elliptical molds)

3.3 Preparation of PLA diffraction gratings

After obtaining the PDMS intermediate molds, the PLA thin films with diffraction gratings were prepared in a second templating process. To prepare the solution, 1g of washed PLA pellets were dissolved in 200 mL of dimethylformamide on a hotplate at 120°C. The solution was returned to room temperature and 30 µL were poured over the 1 cm^2 PDMS intermediate mold and allowed to dry on a hot plate at 110°C, Figure 3.2. After the solvent visually appeared to be dry on the hot plate (approximately 10 minutes), the samples were left on the hot plate an extra 30 s and then removed. All PDMS/PLA samples were dried at room temperature and atmospheric pressure for at least 7 days before separating the PLA from the PDMS intermediate mold. Before separation, the PLA films were cleaned with isopropyl alcohol, and a transparent, double-sided adhesive tape was applied to the PLA. The PLA films were then carefully peeled from the PDMS and mounted in polystyrene cuvettes.

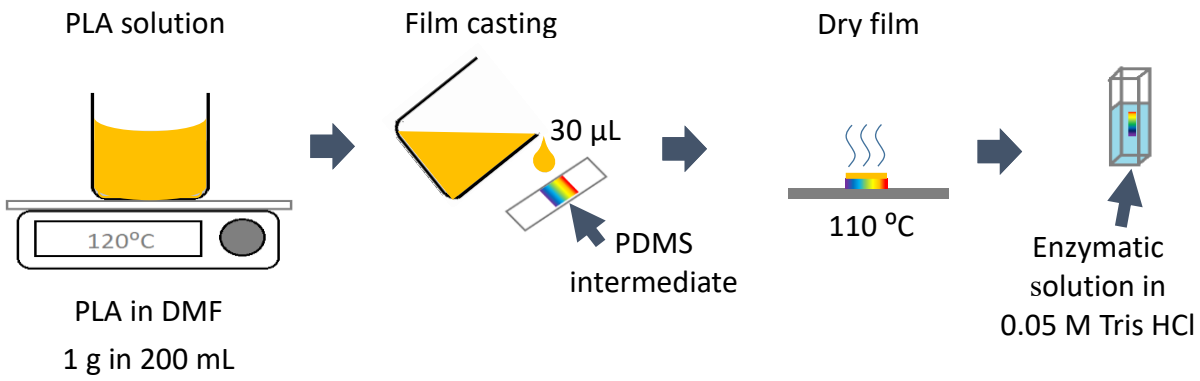

Figure 3.2. Double template process for patterned PLA film preparation.

3.4 Enzyme solution

The degradation solutions varied in different parameters: enzyme concentration (150 µg/mL, 200 µg/mL and 300 µg/mL), temperature and pH. These proteinase K solutions with a variety of conditions were used to degrade PLA films.

First, we prepared a highly concentrated stock solution dissolving 100 mg of proteinase K in 10 mL of storage buffer. The storage buffer was made by mixing 1 mL of 1M Tris-HCl at pH 8, 5 mL of glycerol, 0.29 mL of $CaCl_2$ and 3.71 mL of deionized H_2O, and it was stored at -20°C in 0.5 mL aliquots. Depending on the enzyme concentration required, we took an aliquot of the stock solution to obtain 60 µL, 80 µL or 120 µL. After obtaining this specific volume of

the enzyme solution, we dissolved it in a different buffer with pre fixed pH. These buffers were 0.05 M Tris-HCl with different pH. Each buffer was previously modified with different quantities of 1M NaOH or 1M HCl to reach the pH desired values (pH 6, pH 7, pH 8, pH 9 and pH 10). To form the degradation solutions, the required volume of proteinase K storage solution was diluted in a specific volume of one of the 0.05 M Tris-HCl buffers with the fixed pH to reach the concentration desired (3.94 mL, 3.92 mL or 3.88 mL, depending the concentration). The buffers with the required pH were heated to the working temperature.

3.5 Film characterization

The crystallinity of the films was determined by differential scanning calorimetry (Flash DSC Model 1, Mettler-Toledo, Canada). This thermal analysis was performed from -10°C to 210°C, using a heating rate of 10°C/min, with approximately 5 mg of sample under a nitrogen flow of 20 mL/min.

The films were also evaluated with a UV/Vis spectrophotometer (Hitachi U-3900H) from 200 nm to 650 nm in transmission mode with a scan speed of 60 nm/min, a sampling interval of 0.50 nm and a slit width of 2 nm.

The surface morphology of the different films, before and after specific degradation times, was characterized using a Bruker Nano Dimension Edge atomic force microscope (AFM). The equipment was used in tapping mode using a tip with a spring constant of 42 N/m. The 10 µm × 10 µm images and the profiles of PLA films were processed using NanoScope Analysis Software (Bruker Corporation).

3.6 Optical diffraction setup

As shown in previous work [14], the diffraction-based degradation sensor involves a Class IIIb 532 nm laser, (ARIES #GAR050XXX, Laserglow technologies) as the light source, the PLA thin film with its patterned surface and photodetectors (Wand UV/VIS Quantum #1212310, Coherent) to measure the beam intensities. The total laser power output was ~43 mW, and a glass beamsplitter was used to divide the laser intensity into sample and reference paths (84:16 ratio). The reference photodetector was placed 20 cm ± 0.5 cm from the beamsplitter, and the sample photodetector was placed at a distance of 15 cm ± 0.5 cm from the sample cuvette and aligned to receive the first-order diffracted beam. The reference data was collected at the same time as the main beam. This data was used to obtain information about the

laser stability. The reference beam data was used in the calculations. The experimental value at a specific time was divided by the specific reference value at that point then multiplied by the average of the reference values over the entire experiment (to reintroduce the units and magnitude of the intensity). By including this data, the experimental data considered the laser fluctuations.

Enzymes are highly sensitive to their environment and can be deactivated for contaminants, for this reason the cuvettes and the films were sprayed with IPA and allowed to dry prior to diffraction-based degradation experiments to avoid impurities. The diagram of this setup is shown in Figure 3.3. The sample cuvette was partially immersed in an oil bath to keep the temperature of the degradation solution constant, and the oil bath temperature was continuously monitored with the hotplate's adjunct thermocouple. All the measurements were made in darkness. Additionally, the cuvette was firmly fixed by one clamp to keep the position and a bar on top also fixed, to avoid perturbations during the experiment. PowerSource software (Coherent Inc.) was used to collect the data. Data points were acquired every second, and 5 min of recorded data were averaged for every data point presented in the plots. The intensity curve used at least three different intensity measurements averaged and plotted against degradation time. Hence, the diffraction-based degradation method captured the intensity data from the first order diffraction beam as time passes.

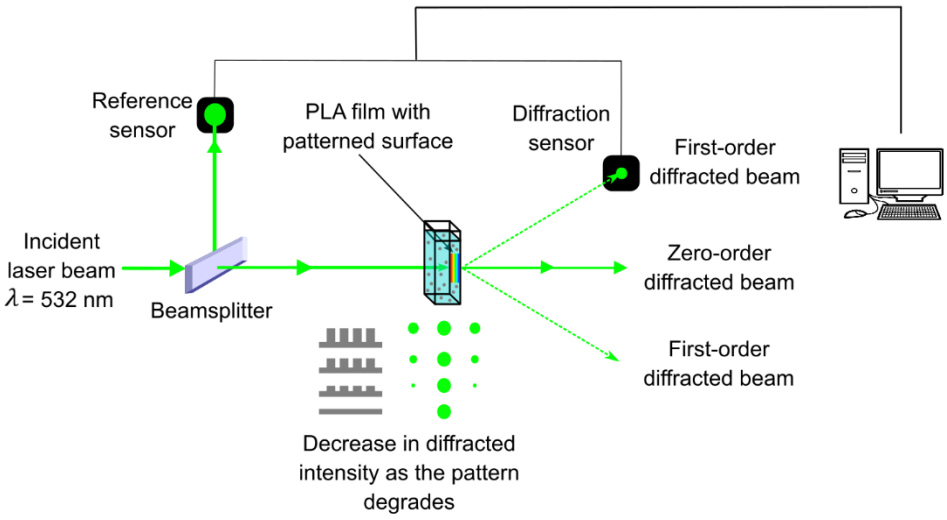

Figure 3.3. Experimental set-up and operation of the diffraction-based degradation sensor. The PLA thin film with the diffraction pattern is placed inside the cuvette with the enzymatic solution. The laser beam irradiates the surface of the film and it is diffracted by the grating. The first-order diffraction spot is measured by a photodetector that acquires data every second.

3.7 Optimizing beam spot for PLA films with elliptical gratings

Triangular PLA films had a regular diffraction grating throughout their entire surface. However, due to fabrication characteristics of the elliptical molds, PLA films with elliptical gratings presented an irregular diffraction grating. To ensure the optimum position was studied, the PLA films with elliptical gratings were mapped. The area of the films was first divided into nine regions, and we selected the region producing the maximum first order diffraction intensity. Once this area was located, we made nine more sub-divisions, marking the lowest and the highest intensity obtained. The diagram that shows how the mapping was made is presented in Figure 3.4. Subsequently, the selected areas of the PLA films with elliptical gratings were analyzed by AFM, and the region that showed the highest intensity was selected to perform the degradation tests.

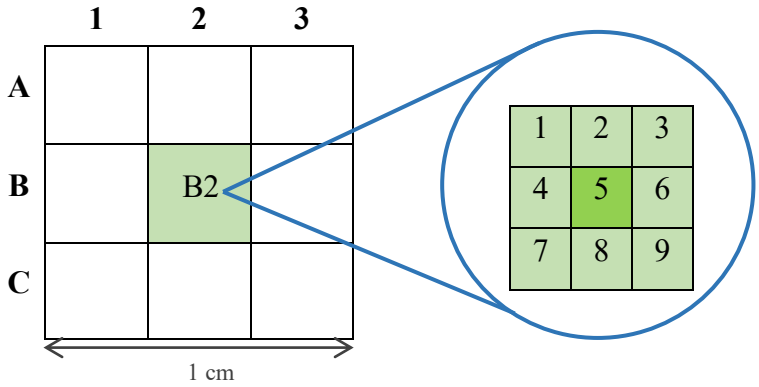

Figure 3.4. Mapping of PLA films with elliptical gratings

3.8 Simulations

OmniSim version 6.2 (Photon Design) is a software package that enables the design of virtual photonic components like ring resonators or gratings. This simulation package includes a highly efficient optical calculation engine that simulates the propagation of incident light through the designs. The modelling of gratings is made under certain assumptions like uniformity in the y-direction when the geometry is defined in ZX plane, and periodicity along the z-direction. It is also possible to define the input beam, changing the polarization of the plane wave and its direction [96]. Some available results of this software are the electromagnetic fields inside the structure of the grating, absorption profiles and effective indices in each layer, as well as the power, phase, direction and propagation constant of the diffraction orders in transmission or reflection modes [96]. The optimization routine takes into account the structure

used in the experiments identifying 3 different regions: the cover region, the grating region and the substrate region [96], [97]. For the cover region, the refractive index was fixed at 1.33, since the gratings are immersed in aqueous solution during degradation, while for the other regions, we use n=1.5 (PLA refractive index). The geometrical characteristics of the gratings such as height, width, substrate thickness and degradation structure changes (variable grating height with fixed grating width) are shown in Figure 3.5.

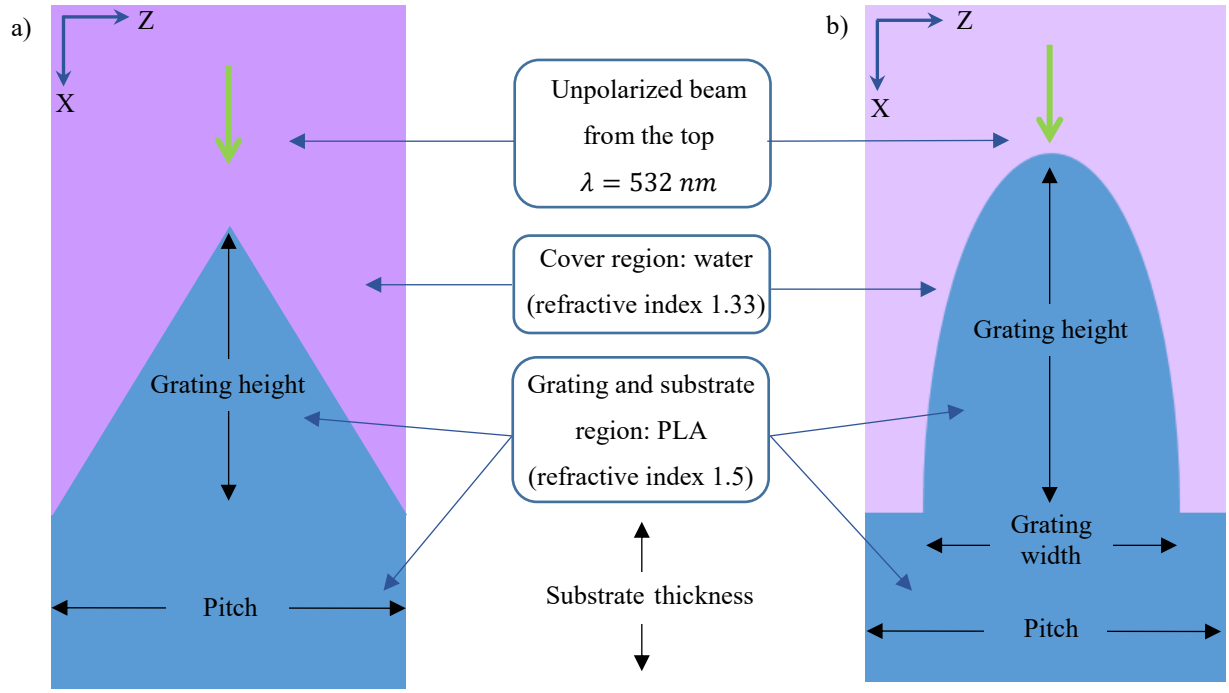

Figure 3.5. (a) Triangular and (b) elliptical grating geometries with the variables used in the simulation

After defining the geometry, the simulation uses rigorous coupled-wave analysis (RCWA) to obtain the fraction of the incident light transmitted in the first diffraction order. In the specific simulations, certain parameters were specified: MaxLayers=20, NZ=40, NThreads=2, and FFactorization=NVF. MaxLayers is used when the geometry varies along the direction of light propagation discretizing the structures into this number of layers. NZ sets the resolution of the engine since it is the number of modes used in the simulation. NThreads is fixed as the number of physical cores on the computer; and NVF is a normal vector field method, a Fourier factorization method optimized for non-rectangular geometries. The incident beam was an unpolarized 532 nm plane wave of arbitrary intensity, and the simulation output was the fraction of this incident intensity transmitted as the first order diffraction. This software provides

information about the measurement of the transmitted power (intensity) in the first diffraction order and allows a plot of normalized intensity vs. height to be constructed.

4. Results and discussion

4.1 Surface and profile characterization

In this work, I used a well-established microfabrication method to replicate the geometry of a diffraction grating. I accomplished this by transferring the geometry from a master mold to a PDMS intermediate mold and subsequently to a PLA film.

The master mold used for most experiments was a diffraction grating made of a polymer coating on top of a glass substrate (ordered from Edmund Optics, New Jersey, USA). This triangular master mold was delicate and needed to be handled carefully to avoid any damage on its surface [75]. For this reason, I prepared an intermediate mold that I used instead of the master mold. The intermediate mold was fabricated using a flexible and well-understood material, polydimethylsiloxane (PDMS). After fabricating the PDMS intermediate mold, I used it to prepare PLA films that were cast on the PDMS intermediate mold.

In Figure 4.1, I present the surface characterization of the triangular master mold, the PDMS intermediate mold, and the PLA films. It was essential to maintain the same features since the optical outputs of the diffraction grating are determined by the geometry of the features [14]. If any of the features change, the diffraction pattern would change, and interfere with the repeatability of the experiments. Figure 4.1 (a) presents the top view of the three surfaces' morphologies obtained by AFM. The 10 μm x 10 μm images show the characteristic straight lines corresponding to the peaks and valleys in the diffraction gratings. The triangular master mold surface is uniform while the PDMS intermediate mold surface exhibits small irregularities. However, the geometries of the PDMS replica and the PLA film are only slightly different from the original master mold.

Figure 4.1 (b) shows the profile pattern of the master triangular mold, the PDMS triangular intermediate mold and the PLA films. This figure shows the profile pattern characteristics were well transferred from the triangular master mold to the triangular PDMS intermediate mold and to the PLA films. From these profiles, I could obtain height, pitch and width measurements. The master triangular mold had nominal factory features of 650 nm height and 1.66 μm width. These dimensions were consistent with those measured by AFM: a height

of 640 ± 22 nm (n = 5) and width of 1.64 ± 0.2 µm (n = 5). The height and width of the PDMS intermediate mold were 633 ± 25 nm (n = 5) and 1.63 ± 0.1 µm (n = 5) respectively. The height and width of the PLA film were 628 ± 12 nm (n = 5) and 1.60 µm ± 0.3 µm (n = 5), respectively. The dimensions of the PDMS intermediate mold were slightly less than those of the triangular master mold. However, the overall quality found on the PDMS intermediate mold is acceptable. Furthermore, the dimensions of the PLA films were also minimally different from the ones obtained of the PDMS intermediate mold.

These variations can be attributed to air bubbles trapped in the smallest features, which can interfere in the replication of these characteristics [98]. Additionally, the replication process is determined by wetting, Van der Waals interactions, and the filling of the mold [99]. In this work, I did a second degassing in the vacuum chamber after pouring the PDMS (described in Chapter III). However, it is still possible to observe differences that can be ascribed to impurities on the surface or possibly defects introduced when the mold is removed. These images suggest that the morphological features of the master triangular mold were well transferred to the intermediate mold and finally to the PLA films which agree with the studies regarding current methods on microfluidic fabrication [100]. The results I obtained by using a replica-mold process agree with the literature where it has been demonstrated that up to seven polymer replicas can be formed from PDMS molds without deformation [2].

Figure 4.1 (c) shows a 3D image of the PLA film surface, which demonstrates that mold-replica separation followed by a solvent-casting process, is a viable option to obtain PLA films with the triangular master mold characteristics from less delicate PDMS intermediate molds.

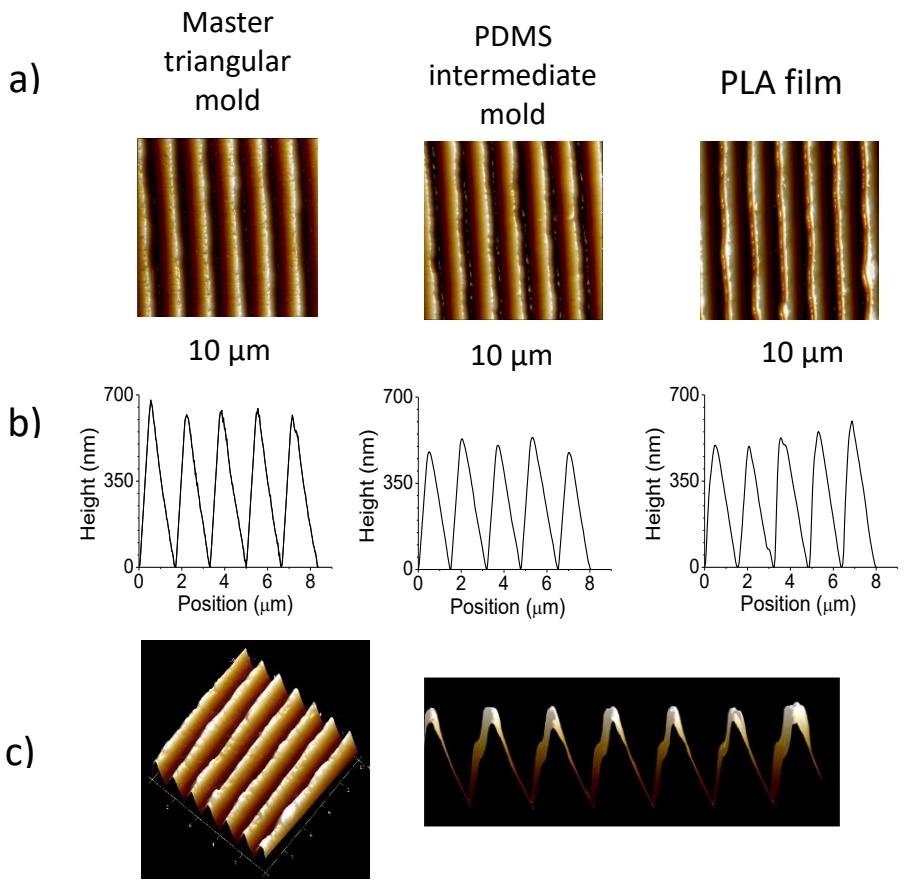

Figure 4.1. a) AFM images detailing the surface morphology of the triangular master mold, the triangular PDMS mold and the triangular PLA film, each image corresponds to 100 μm^2 . b) The associated 2D line scan profiles for each sample and c) 3D images of the surface of the PLA film obtained by AFM

4.2 Enzymatic degradation of triangular PLA films

Polymer films with gratings were immersed in enzymatic solution while the intensity of the diffracted beam was measured to study and monitor the enzymatic degradation of PLA.

Within this setup, the laser was divided into sample and reference paths using a beam splitter with a ratio of 84:16. The laser had a total output of 43 ± 3 mW $(n = 5)$ and only being divided by the beam splitter, the intensity registered immediately before the grating was 36 ± 2 mW $(n = 5)$. The reference beam presented a value of 6.4 ± 0.5 mW $(n = 5)$, and for the first-order diffraction beam intensity the value was 13.9 ± 0.1 mW $(n = 5)$. This data is also presented in Table 4-1. The different intensities obtained are due to the geometry of the diffraction grating. This grating is a blaze angle type designed to maximize the intensity in a specific order while minimize the residual power in the rest of the orders.

Table 4-1. Intensities collected at different points

Position	**Intensity**
Total output	43.76 mW
Reference beam	6.4 ± 0.5 mW
Cuvette input	36 ± 2 mW
0 order diffraction beam	6.7 mW$\pm$.6 mW
1st order diffraction beam	13.9 ± 1 mW
-1st order diffraction beam	3.18 $\pm$0.6 mW
2nd order diffraction beam	216 $\pm$10 μW
-2nd order diffraction beam	2.11 ± 0.1 mW

Among other factors, enzymatic activity is affected by temperature, enzyme concentration and pH; to obtain the maximum enzymatic activity, the films were immersed in solutions with different enzyme concentrations at different values of pH and temperature. The pH varied from 6 to 10, the concentration from 150 to 300 μg/mL, and the temperature from RT to 60°C. In addition, control samples of PLA immersed in buffer with no enzymes were evaluated.

Figure 4.2 shows plots with the degradation time in the x-axis and normalized intensity of the diffracted laser beam in the y-axis, for all sets of conditions. In Figure 4.2 (a), I present the control solution comprised of a buffer with no enzyme under the same conditions of temperature and pH. This control is a straight line, showing there were no changes in intensity over time. This constant intensity suggests the PLA film was not affected by exposure to the buffer, meaning the polymer films are stable under these conditions. For clarity purposes, this control experiment is only shown in Figure 4.2 (a).

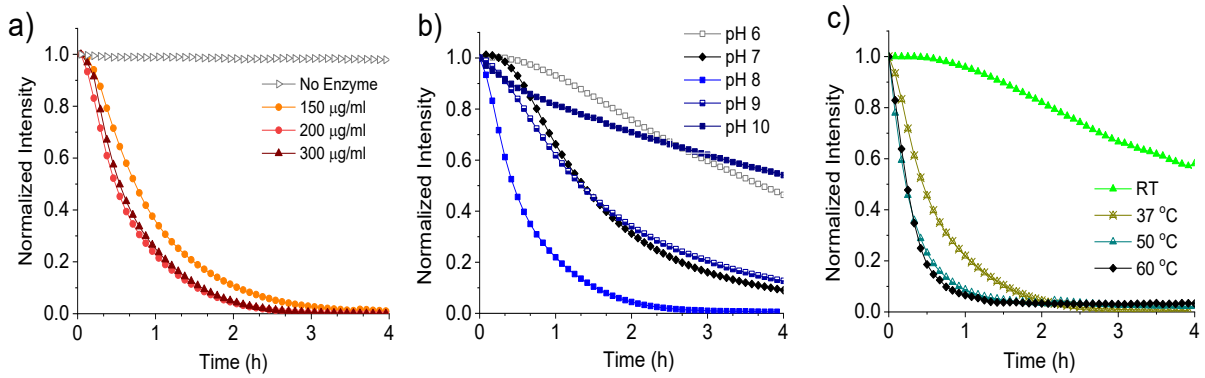

Figure 4.2. Evolution of the intensity of the first-order diffraction spot for triangular PLA gratings degrading under a variety of conditions: a) different proteinase K concentrations at 37°C and pH 8, b) different temperatures with pH 8 and 200 µg/mL proteinase K, and c) different pH from pH 6 to pH 10 at 37°C and a proteinase K concentration of 200 µg/mL.

Figure 4.2 (a) shows the evolution of the intensity of the diffracted beam exposed to different concentrations of enzyme maintaining a constant pH 8 and a temperature of 37°C. The different concentrations studied were 150 µg/mL, 200 µg/mL, and 300 µg/mL. In the three cases, there is a faster decay during the first hour, a decelerated degradation rate from 1 to 3 hours then a plateau from 3 hours to 4 hours. When the plot shows a 0% intensity, the diffraction pattern disappeared, and there is no longer a diffracted beam to track. The plateau indicates this absence of a diffracted beam during the last hour of the experiment. The behavior of the intensity with concentrations of 200 and 300 µg/mL are similar.

The trend shows that increasing the concentration from the lowest concentration (150 µg/mL) improved the speed of reaction, reaching an optimum behavior at 200 µg/mL and maintaining at 300 µg/mL. This similar change in intensity for 300 µg/mL may be caused by a saturation of the available substrate (polymer) for the enzymes to bind to [53]. This suggests that at 300 µg/mL there was no longer accessible substrate for the enzyme to bind to, possibly causing the rest of the enzyme to remain in the solution rather than attached [4].

Figure 4.2 (b) shows the progress of the enzymatic degradation when pH varies within the region of activity for proteinase K (pH 6 – 10). The curves changed for each pH, for pH 8 there is a faster decay during the first hour, reaching a normalized intensity of 0.2. For pH 7 and pH 9, the behaviors are similar: the decaying intensity profile also appears, however after the first hour they showed a normalized intensity of 0.6, and they do not reach zero within the four-hour period of the experiment. This suggests that the enzyme did not fully degrade the surface

pattern. For pH 6 and pH 10, throughout 4 hours of the experiment, there is a decreasing intensity profile with a lowest value of approximately 0.4.

The pH 8 profile showed the fastest degradation rate suggesting that the optimum pH for proteinase K activity was pH 8. Higher or lower values decrease the enzymatic activity and the degradation reaction velocity [53]. At values slightly different than pH 8, i.e. pH 7 and pH 9, the enzyme properties are suboptimal, lowering the reaction rate. Regarding pH values of 6 and 10, the dramatically reduced degradation rates can be caused by changes in the protein conformation [102]. The slower degradation could also be caused by modifications from the optimum pH that can cause the formation and breakage of intramolecular bonds. These conformational changes modify the shape of the protein, changing the active site in the catalyst which decreases the activity for most enzymes [54].

In Figure 4.2 (c), the PLA degradation rate was studied at a constant pH 8 and a concentration of 200 μg/mL while varying the temperature within the working enzyme range [48]. The curve corresponding to room temperature (RT) presents a plateau during the first 40 minutes, followed by a decrease that after 4 hours of experiment, reached a normalized intensity of 0.6. In this graph, the curves corresponding to 50°C and 60°C presented a steep decrease of intensity during the first 30 minutes of enzymatic exposure, reaching 0.05 of normalized intensity by the first hour. However, both curves maintained this constant value, and do not reach zero intensity with the 4 hours of the experiment.

Temperature effects in enzyme behavior are not simple. As the temperature is raised, the rate of reaction increases, which can be observed in the plots corresponding to 50 and 60ºC. This increase is probably due to that the reacting molecules are gaining kinetic energy, causing a faster degradation rate during the first hour [53]. However, there is also a progressive inactivation caused by intra- and intermolecular bonds broken in the enzyme [54]. Thermal denaturation depends on time, and this deactivation is observed in the plateau at 0.05 after 1 hour. This thermal stability has been studied for proteinase K and agrees with our results [48].

From the plots in Figure 4.2, the derivatives of intensity with respect to time were calculated and are plotted against time. These graphs are shown in Figure 4.3. In Figure 4.3 (a), the differential curves for different concentrations are shown. The graphs present a marked slope that reached a minimum around the first 20 minutes, this change refers to the initial decrease in intensity. After this dip, the change in the rate from 20 to 60 minutes for the three concentrations

is becoming closer to zero. Around 2 hours, the changes in the degradation rate are minimum without reaching the zero value, which can represent a constant but minimal decrease in this rate. The results corroborate that the fastest degradation process occurs at the concentrations of 200 µg/mL and 300 µg/mL, with a change of -0.025 in intensity per hour around 20 minutes. Figure 4.3 (b) shows the effect of pH on degradation rate. While pH 8 provides the fastest decay in intensity during the first 15 minutes, pH 7 presents a decay around 45 min. Meanwhile, pH 9 shows a broad curve that starts increasing after around 40 minutes. Regarding the pH 6 and 10, they present irregular intensity decays, which can suggest other factors are influencing the decrease in intensity or that these factors may need a longer exposure time to be observed. In these plots, pH 8 is the only one that reaches zero, which indicates no further changes in the intensity. The rest of the curves still present non-zero derivatives after four hours.

In Figure 4.3 (c), it is possible to observe the curves corresponding to RT, 37°C and 60°C present a dip while the curve of 50°C does not. Additionally, the fastest degradation occurred at 50°C; at this temperature, there was no initial rate increase, which could be caused by the speed of reaction exceeding the equipment's ability to record data. The plot for temperature of 60°C presents an initial increase followed by the decrease in the degradation rate at 6 minutes. Both higher temperatures (50°C and 60°C), reached a plateau around zero µW/min at approximately 90 minutes. However, these plateaus do not correspond to complete disappearance of the diffraction grating, which was still detected by our setup, but they can apply to denaturation of the enzyme by prolonged exposure to these temperatures [53]. There exist several works that provide information about the unfavorable effects of high temperatures in enzymes [53], [103], [104].

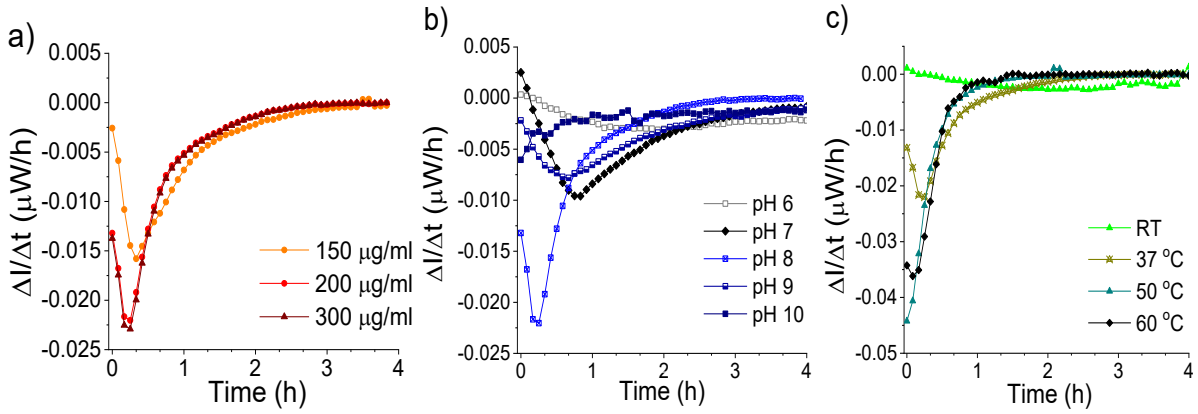

Figure 4.3. Derivatives of curves shown in Figure 4.2, representing rate of intensity change as a function of time under a variety of conditions: a) different proteinase K concentrations at 37°C and pH 8, b) different temperatures with pH 8 and 200 µg/mL proteinase K, and c) different pH from pH 6 to pH 10 at 37°C and a proteinase K concentration of 200 µg/mL.

This method tracked the influence of different conditions for the catalyzed hydrolysis of PLA in the presence of a protease. These changes were a result of modifications of the degradation environment like pH, concentration and temperature. As expected, each parameter had a different effect on the process, and these experiments were made to prove the method was able to track the changes caused by the different variations. In this work, the diffraction-based method was able to show the optimum conditions for PLA film degradation were pH 8, 200 µg/mL at 37°C that agrees with the literature [104], [105].

Once I obtained the optimum conditions where the enzyme did not suffer any deactivation and presented a suitable reaction rate, I wanted to elucidate if periodically refreshing the enzyme solution would affect the degradation rate, and the results are shown in Figure 4.4. The enzymatic solution was changed every 30 minutes, each time replacing the spent solution with a fresh but otherwise identical solution. The slight change in the curves corresponds to the time the old solution was removed and replaced for a new solution. However, the introduction of new enzymes did not affect the intensity results. Yamashita et al. have shown that proteinase K apparently adsorbs irreversibly from PLA films surfaces [101]. The fact that the intensity remained immutable despite the solution changes can be caused by the adsorbed enzymes from the old solution already occupying the binding sites, and not being easily released [101]. This has been observed in previous work of PLA enzymatic degradation where the film degradation stays at the film surface, and the enzyme cannot diffuse into the bulk material [106]. Since degradation preferentially happens in amorphous sites, after the initial degradation, there

are only crystalline sites, and enzymes did not attach to these areas, which does not affect the initial degradation rate [107].

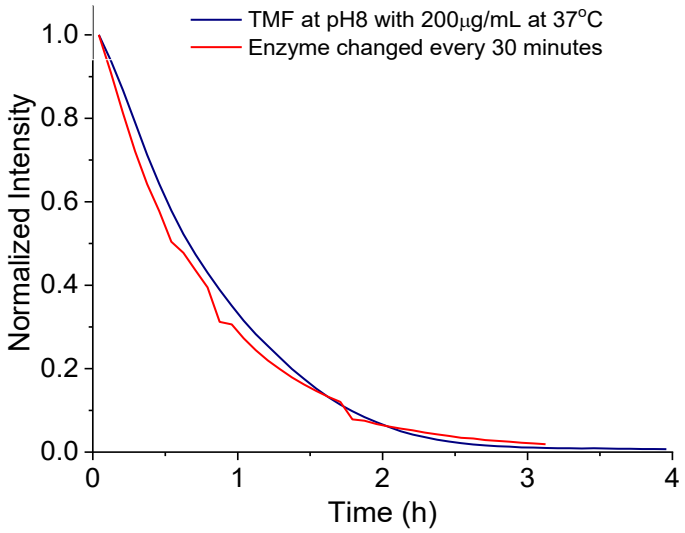

Figure 4.4. Normalized intensity versus time of PLA triangular master film (TMF) under pH 8, 200 μg/mL at 37°C for 4 hours and the enzyme solution changed every 30 minutes.

4.3 Diffraction efficiency and surface profile

To study the change in shape of degradable diffraction gratings during degradation experiments, PLA films with triangular diffraction gratings were exposed to the optimum degradation conditions identified in section 4.2. The enzymatic degradation process was interrupted at specific times; then the partially-degraded samples were washed and analyzed by AFM to track the changes in the surface profiles. The progress of the enzymatic degradation was stopped at 15 min, 30 min, 45 min and 60 min since the fastest decay in intensity was observed during the first hour of the experiment. After one hour, the data density was reduced, and samples were produced after 120 min, 180 min and 240 min of degradation in enzymatic solution. Several AFM images are presented in Figure 4.5.

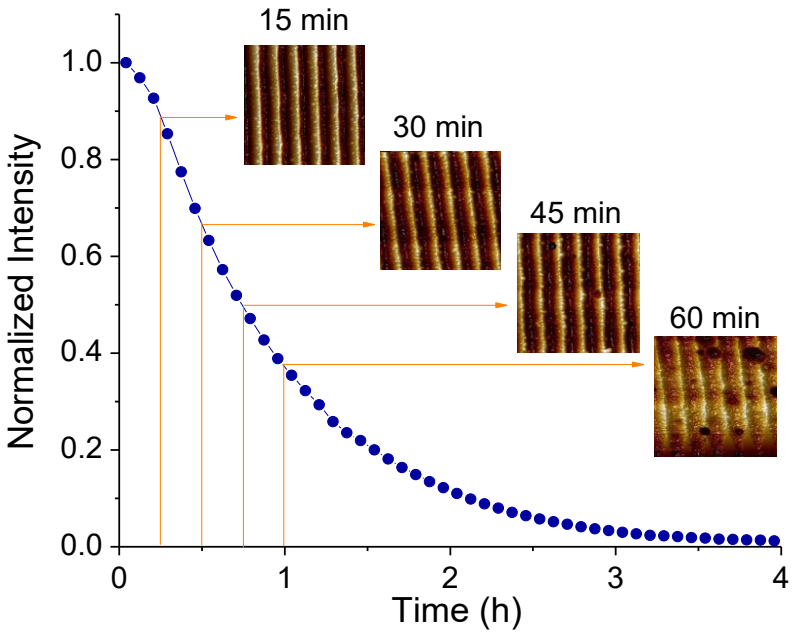

Figure 4.5. The plot of the first-order diffraction intensity vs degradation time for a triangular PLA grating under optimum degradation conditions. AFM images of representative samples exposed to the optimized conditions are included as insets.

In this figure, it is possible to observe that at 15 minutes, the PLA diffraction grating still presents the parallel straight lines characteristic of the original pattern. However, the surface of this sample starts showing small irregularities. At 30 minutes the lines are broader, but the surface is generally uniform with the presence of some defects. The image at 45 minutes started showing some pits in the PLA surface, and the lines are not as thin as before, while the film exposed for 60 minutes presents several defects in its surface. Even when the grating lines are still visible, they are wider than the 45 minutes samples. The sample at 0 minutes clearly shows the characteristics of 628 nm ± 19 nm (n = 5) in height and width of 1.60 µm ± 0.5 µm (n = 5). The samples at 15, 30 and 45 minutes present the same shape as the non-degraded film. For the height characteristics, the measurements were 520 nm ± 35 nm (n = 5), 470 nm ± 23 nm (n = 5), and 429 nm ± 42 nm (n = 5) for the 15, 30 and 45 minute samples, respectively. The corresponding widths for these samples are 1.59 µm ± 0.3 µm (n =5), 1.60 µm ± 0.1 µm (n = 5) and 1.6 µm ± 0.03 µm (n = 5). For the sample at 60 min, the height is 354 nm ± 34 nm (n = 5), and the pitch is maintained at 1.6 µm ± 0.8 µm (n = 5).

The geometrical changes occurring within the first 30 minutes can be caused by the initial stages of degradation [34]. The degradation process generates irregularities as a consequence of the enzymatic attack [106] [108]. The visible changes at 45 minutes indicate

the enzymatic attack is occurring [51]. Finally, at 60 minutes, the degradation process is evident with the formation of deep holes, cracks and fragmentation along with surface roughening, which are all characteristics of plastic degradation through heterogeneous surface erosion [39], [51], [109].

In order to understand the degradation process, the changes in the size and height were estimated by cross-section AFM analysis and they are shown in Figure 4.6 (a). As a comparison, the lines at different degradation times are shown in Figure 4.6 (b). The height measurements presented before degradation are complemented by the rest of the films observed at 120, 180 and 240 minutes. The film for which the degradation process was interrupted at 120 minutes presents a height of 239 nm ± 58 nm (n = 5), with a pitch of 1.6 μm ± 0.5 μm (n = 5). The sample interrupted at 180 min is the last sample that still presents the peaks. However, the height is reduced to 173 ± 65 nm (n = 5), and the pitch is now harder to define. The gratings deteriorate until they are no longer distinguishable at 240 minutes of exposure to the enzymatic solution. At this time, the diffraction grating is entirely gone, while voids and fissures of a greater size than the original grating features appear across the sample.

PLA enzymatic degradation by hydrolysis is a complex process [49], [110]. The multi-step process is characterized by enzyme diffusion to the solid surface, followed by enzyme adsorption through the surface-binding domain [49]. Subsequently, the enzyme catalyzes the cleavage of main chain ester bonds, causing the separation of oligomers and monomers from the backbone chain [49]. The separation of these soluble degradation products can produce surface roughening over time, which agrees with the AFM images [111].

PLA is well known for undergoing bulk erosion [112]. However, Grizzi et al. have shown that small PLA devices such as films and microspheres degraded differently from their larger counterparts [113]. These results agree with shorter degradation times, depending on the size of the item [49]. As mentioned in other works, the enzymatic degradation is affected by the amount of crystallinity in the samples [114]. In this work, PLA films were characterized prior the experiments by DSC analysis. From these studies, the samples presented a crystallinity of 11% calculated from the results (see Appendix A: Additional Results, for figures containing DSC curves and the information from PLA films casted at different temperatures).

Additionally, it has been demonstrated that enzymes generally preferred to attack the amorphous regions first, which can explain the creation of holes in specific sites on the surface

[17], [24] [26]. These areas were probably more accessible to water molecules and enzymes due to the lack of structure that hindered the adsorption of proteinase K [106], [107], [110].

These profiles show that as time passes, the diffraction gratings undergo surface erosion. These irregularities are indicative of polymer degradation that increases surface roughness [115]. Enzymatic degradation is a process where the material is degraded from the surface inwards, mainly because the macromolecular size of the enzyme prevents diffusion into the interior of the material. This has been shown in other works where the dimensions of the proteinase K control its diffusion [106], [116]. This can be observed based on the geometry during the degradation process. The profiles demonstrate the peak heights diminish while the widths are maintained over time. This can be caused by the peaks being attacked by both sides. These areas are more exposed to the enzymatic attack while the bottom area is harder to reach. This phenomenon has also been observed in microelectronics, where the geometry influences the etch rate of structures.

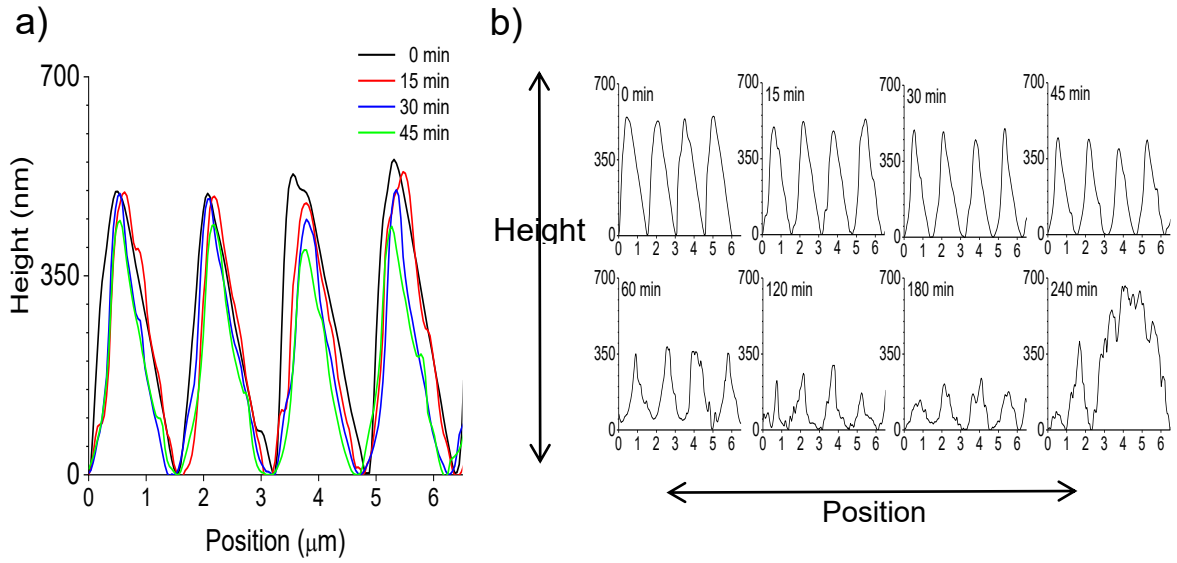

Figure 4.6. AFM line profiles of triangular PLA gratings exposed for different lengths of time to the 200 μg/mL proteinase K solution at 37°C and pH 8. The first four lines scans are displayed together on a single set of axes in (a) for comparison purposes. Each plot of the gratings exposed to different degradation times is presented in (b).

These results demonstrate that as the PLA gratings are immersed in degradation solution the gratings diminish in height. Since previous results indicate that the diffracted intensity decreases with time spent in the degradation solution, the height is related to the intensity which agrees with the work reported by other authors [75]. PLA films studied here present a surface

erosion degradation process [112]. In this case, due to the dimensions of the thin film, I observed a heterogeneous rather than homogeneous erosion [115], [117]. This change agrees with the work of Grizzy et al., where the PLA degradation behavior changes as the sample size is reduced [113]. Furthermore, these results relate to the intensity changes with a degradation process.

4.4 Simulation of diffraction for triangular gratings

OmniSim software provided theoretical information of intensity versus height. By using this software, it can be possible to relate experimental results of intensity versus time to a specific height without needing further characterization to obtain the grating height. Thus, this simulated data not only can provide quantitative information of the degradation of polymer thin films but another characterization method for minuscule structures.

A theoretical plot of intensity versus height was obtained using the simulation software. The geometry of the simulated grating was chosen to match the observations from the AFM experiments. One of the parameters introduced in this simulation was a grating height that varied throughout the experiment. The rest of the parameters like pitch (1.66 μm), refractive index ($n_{water} = 1.33$ and $n_{PLA} = 1.5$), and substrate thickness ($n = 1.5$) were held constant. For each height, an individual simulation was run to obtain a theoretical diffracted intensity, and using this information, a curve of intensity versus height was obtained. As control, different sets of simulations with variations in the substrate thickness, and water thickness were run; these factors did not show any influence.

In order to use the simulation data, I used a fitting parameter. This fitting parameter for the triangular master mold simulation was a scaling factor. First, the experimental height with its intensity was interpolated to obtain the corresponding intensity from the values of the simulation, and subsequently, I calculate the difference between the experimental intensity and the simulated intensity. Afterward, using the least squares method with these values, the number that gave us the minimum difference was calculated. This number was the scaling factor that I proceed to use as our fitting parameter.

The result was a plot of intensity versus height, as shown in Figure 4.7 (a). The shape of this simulation data started from 0 to 1, set at 628 nm height. The simulation data fitted the experimental data of heights obtained by AFM images. I used this intensity versus height information to examine how the simulation data fits the experimental data. For each set of conditions, there was an individual least-squares fitting process.

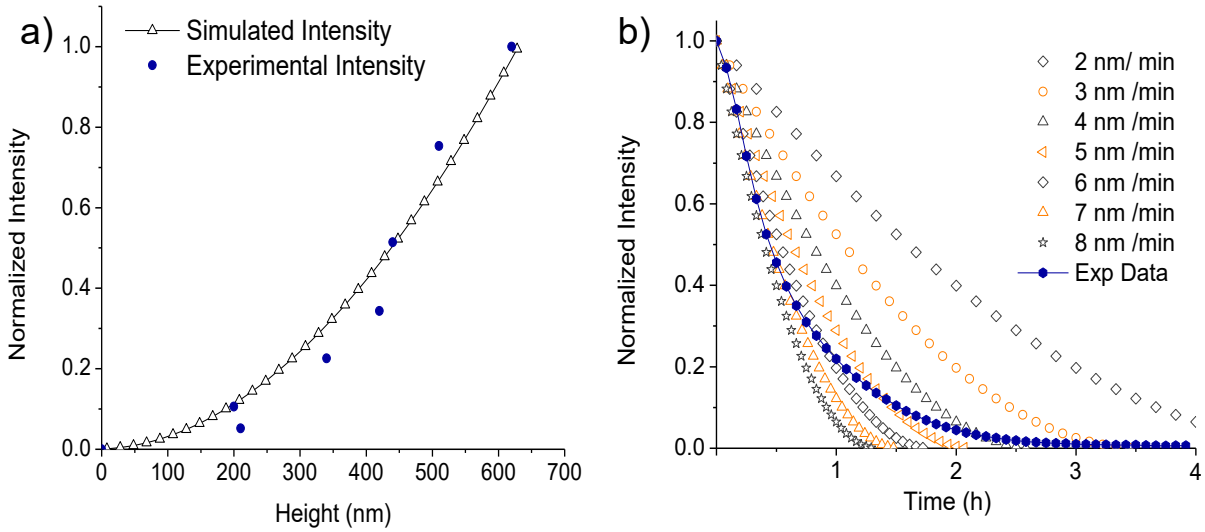

Figure 4.7. a) Normalized intensity versus height plot of experimental data and theoretical data and b) Normalized intensity versus time, comparison of experimental data versus constant etch rates.

The experimental data is intensity vs. time while the simulation data provided a graph of intensity versus height, which is not time based. Hence after obtaining the simulation data, I used equation (1) and by implementing a constant etch rate, I was able to change the 'x' axis from height to time.

$$t_{sim} = \frac{h_{max} - h_{sim}}{v} \tag{1}$$

Where t_{sim} is the time corresponding to the simulation, h_{max} is the maximum physical height, h_{sim} is the height from the simulation software and v is the constant etch rate used to obtain the simulation time.

These constant etch rates, in nm/min, were compared with the experimental data, and are shown in Figure 4.7 (b). The series of datasets presented in this figure, correspond to simulated heights achieved in etch processes where each one had different constant etch rates. The filled blue data points represent an actual experimental curve. At the beginning, the 7 nm/min etch rate fitted the data, nevertheless, after 30 minutes, this fit is no longer adequate to the data. It can be seen the degradation is not occurring at a fixed etch rate. Instead, it appears that the degradation rate is decreasing as time passes. After that, I continue with a second fitting since I was interested in applying this theoretical data to all the conditions studied previously. For this second fitting, I used two new fitting parameters. An initial etch rate and a rate decay constant, which indicate us how much the degradation was slowing. These fitting parameters

were used to calculate the etch rate, since it was not a constant anymore. The new formula for the etch rate is shown in equation (2).

$$v = v_i - d\left(\frac{h_{max} - h_{sim}}{h_{max}}\right) \quad (2)$$

Where v_i is the initial etch rate, d is the rate decay constant, h_{max} is the maximum height and h_{sim} is the height from the simulations.

In order to obtain these new fitting parameters, the process was similar to the first method. The simulated data was obtained from OmniSim software. These theoretical intensities were interpolated to calculate simulated intensities at the specific time points measured with the experimental equipment. Using the least squares method was again used to fit the simulated data to the experimental data, obtaining an initial etch rate with a rate decay constant that minimized the differences between the interpolated simulated data and the experimental data.

Using the simulation intensities, I fitted the experimental data under different degradation environments (i.e., the original data shown in Fig. 4.2) as can be observed in Figure 4.8. The first set of conditions studied was the one corresponding to the different proteinase K concentrations, followed by the pH and the temperatures

In Figure 4.8 (a), it is possible to observe how the simulation data fit the experimental data satisfactorily under the optimum conditions previously obtained in section 4.2. The simulation model fits the experimental data for fairly well, and the fits improved after 30 minutes.

For the case of the experiments under different pH shown in Figure 4.8 (b), the fits obtained by the simulation are better suited for fast degradation and are not able to track intensities that initially increase. For this reason, for pH 6 the values fit better after three hours.

For pH 7, the experimental values present an initial curve during the first hour that does not fit with the simulation data. While for pH 9, this difference is less evident, but it also appears during this time. Finally, for pH 10, the theoretical data agrees with the experimental data throughout the 4 hours. The initial differences observed during different time could possibly be attributed to the phenomenon of proteinase K diffusion and/or adsorption [110]. The environmental conditions during degradation influence the enzyme diffusion and adsorption and these processes may proceed at different rates for each set of environmental conditions

[103]. The enzyme attachment to the polymer surface can be influenced by different pH, which can be observed in this plot.

Figure 4.8 (c) presents the fit curves corresponding to the different temperatures. In the case of room temperature, the simulation data is not able to match the experimental results until 2 hours into the experiment. For the temperatures of 50 and 60ºC, both simulations are almost overlapping each other; they better fit the degradation at 50ºC up to 30 minutes, to present a faster decay after this time. None of the simulations could entirely describe the degradation at 60ºC. Nevertheless, they agree with not reaching zero intensity after 4 hours.

For room temperature, it is possible that due to the non-optimum conditions, the enzyme is suffering various changes. For instance, the temperature might not be adequate to allow the correct diffusion of the enzyme on the surface [110]. Additionally, this temperature can also influence in the adsorption by changing the structure of the enzyme, thus, modifying the formation of the enzyme-substrate complex [110].

Nonetheless, these experiments were carried out at different temperatures, and these modifications may cause that the beginning of the curves did not entirely fit since our model is not expecting variations from the enzyme behavior. It is necessary to mention the sensitivity of enzymes to minimal changes in their environment and enzyme deactivation due to high-temperature exposure [53] [104].

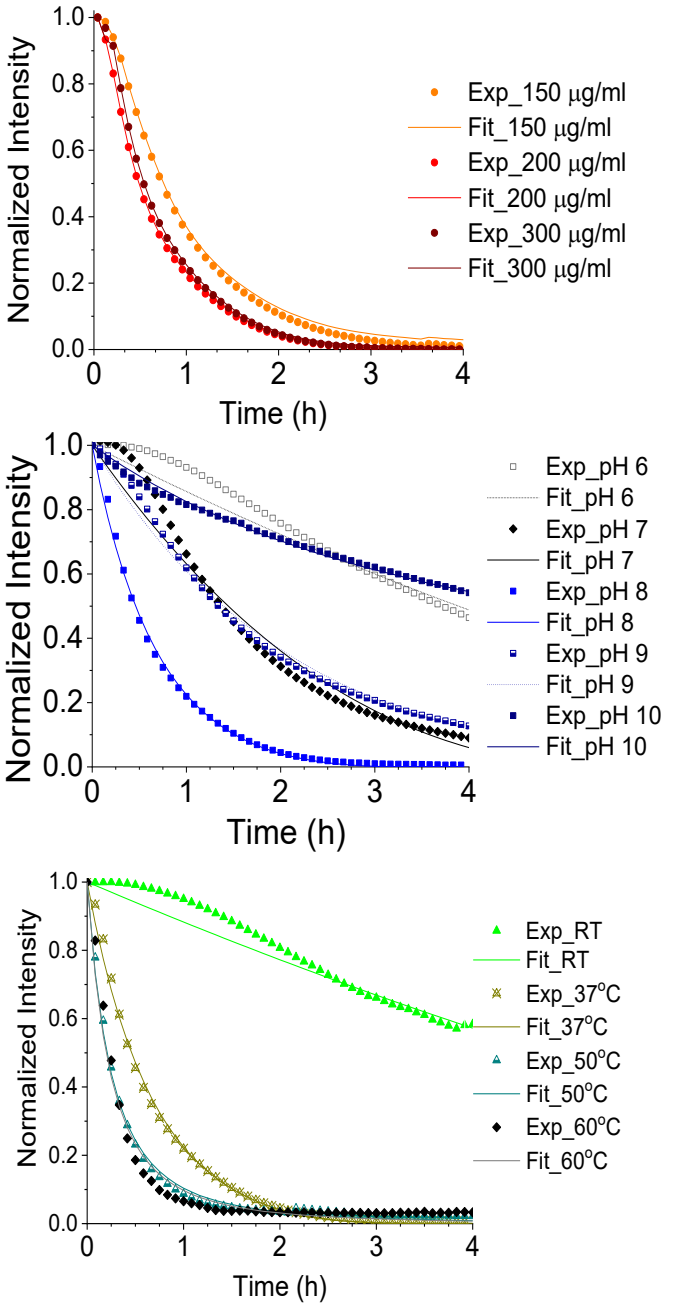

Figure 4.8. Normalized intensity of the first-order diffraction spot for the triangular PLA gratings versus time of experimental and simulated data under different conditions, a) different proteinase K concentrations at 37°C and pH 8, b) different temperatures with pH 8 and 200 µg/mL proteinase K, and c) different pH from pH 6 to pH 10 at 37°C and a proteinase K concentration of 200 µg/mL.

The initial etch rates for each different degradation environment are presented in Table 4-2. The optimum conditions presented an etch rate of 8.5 nm/min. The minimum etch rate obtained corresponded to RT, which is in the limit of the working range of proteinase K [53]. On the other hand, the maximum initial etch rate obtained was the one corresponding to 60ºC,

however, as discussed previously, in this experiment the enzyme stopped working after 1 hour, which indicates enzyme denaturation was taking place [103].

Table 4-2. Initial etch rate obtained by the simulation software

Concentration (µg/mL)	pH	Temperature (°C)	Initial etch rate (nm/min)
150	8	37	5.2
200	6	37	0.8
	7	37	2.3
	8	RT	0.7
		37	8.5
		50	22
		60	22.9
	9	37	2.7
	10	37	1.2
300	8	37	8.4

In Figure 4.9, the graph was built from the initial etch rate values presented in Table 4-2. This plot shows the characteristic shape of the plot of enzyme activity versus pH, showing an optimum etch rate value for pH 8 [53], [103], [118]. This corroborates the hypothesis that the diffraction method was able to provide information about the enzyme behavior and its influence on the degradation rate of polymer thin films.

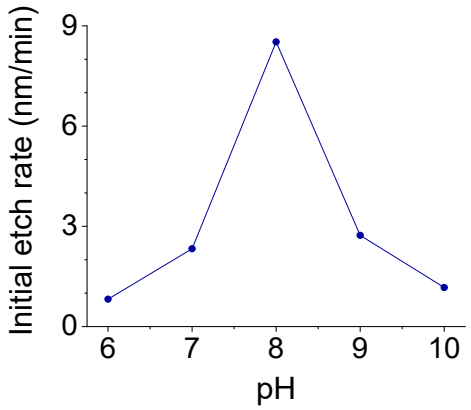

Figure 4.9. Evolution of initial etch rate versus pH

In this section, I obtained simulation data that fitted the experimental values; with this information, I was able to determine initial etch rates. This method was able to provide quantitative information about the degradation of PLA thin films for the different degradation conditions. In other works presented in the literature, there are etch rates proposed. However, they are not focused on 2D films but rather macroscopic structures [119]. Additionally, most of these degradation studies use gravimetric techniques that do not easily apply to films, or they use exhaustive sample preparation and specialised equipment to monitor specific parameters, e.g. molecular weight [119].

4.5 Surface characterization of molds with elliptical gratings

In addition to the experiments done with PLA films with triangular gratings, I observed the evolution of the intensity of PLA films with elliptical gratings to study if the technique is applicable to other geometries. First, these films' morphologies were characterized by AFM. Figure 4.10 shows 10 µm x 10 µm AFM images that present the surface characterization and the cross-section profile of the different PLA films with elliptical gratings ordered by height, with E1 being the smallest and E6 the tallest. E1 showed a height of 110 ± 12 nm ($n = 5$) with a width of 1.07 ± 0.02 µm ($n = 5$). E2, E3, E4, E5 and E6 showed heights of 200 nm ± 7 nm ($n = 5$), 212 nm ± 68 nm ($n = 5$), 287 nm ± 50 nm ($n = 5$), 356 nm ± 37 nm ($n = 5$), and 470 nm ± 9 nm ($n = 5$) respectively. Regarding the widths, the values were 0.97 µm ± 0.03 µm ($n = 5$), 1.1 µm ± 0.04 µm ($n = 5$), 1.09 µm ± 0.01 µm ($n = 5$), 0.99 µm ± 0.04 µm ($n = 5$), and 0.97 µm ± 0.04 µm ($n = 5$) respectively.

Regarding the morphology, they present homogeneous surfaces within the analyzed area, with slight roughness in the higher parts of the structures. These imperfections may be caused by impurities on the mold surface prior to demolding, and can also be attributed to the handling and peeling-off process that can also generate some irregularities on the samples. Replica molding using PDMS has been shown to produce molds with the same quality as the masters and the results obtained show that the characteristics were well transferred using this method, as has been achieved for other materials in the literature [120].

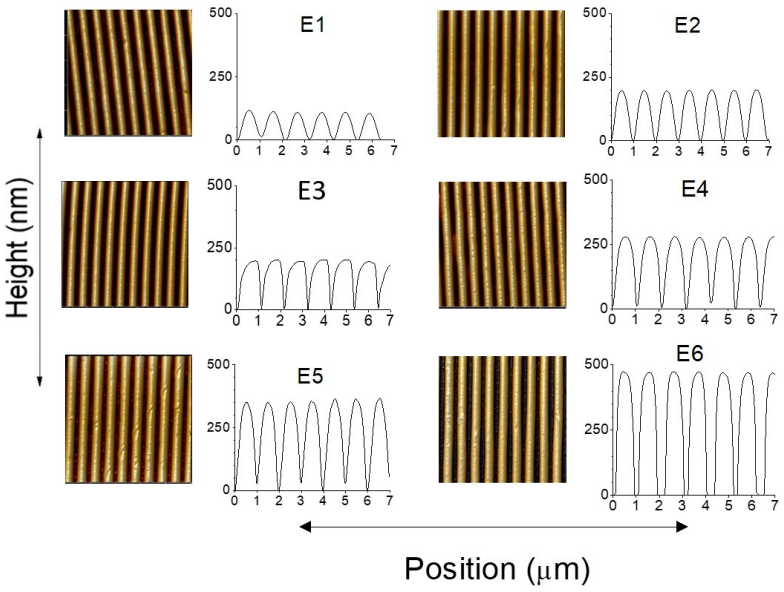

Figure 4.10. Surfaces morphology and cross-sectional images obtained by AFM for PLA films with elliptical gratings

Due to the fabrication process of the elliptical molds made of SU-8, they did not present a constant height across their entire surface, and these height variations were transferred to the PDMS elliptical molds Therefore, it was necessary to track the different intensities along the surface to identify the region of maximum diffraction. The results are presented in Table 4-3. From these results, the increasing heights were related with the increasing intensities obtained. The higher intensities are an average of the same area of five samples taken before immersion. For E1 the maximum diffraction intensity was 1.5 mW ± 0.3 mW ($n = 5$). E2, E3, E4, E5 and E6 showed maximum intensities were 3.26 mW ± 0.4 mW ($n = 5$), 7.3 mW ± 0.43 mW ($n = 5$), 9.3 mW ± 0.31 mW ($n = 5$), 9.33 mW ± 0.47 mW ($n = 5$), and 14.17 mW ± 0.55 mW ($n = 5$), respectively.

Table 4-3. Mapping of PLA films with elliptical gratings

Molds	First Mapping	Mapping in the selected area

E1

	1	2	3
A	.	915 µW	1 mW
B	970 µW	597 µW	890 µW
C	867 µW	**1.11 mW**	298 µW

C2

1 867 µW	**2** 800 µW	**3** 500 µW
4 1.1 mW	**5** 1.5 mW	**6** 500 µW
7 135 µW	**8** 697 µW	**9** 261 µW

E2

	1	2	3
A	2.12 mW	2.98 mW	1.95 mW
B	1.45 mW	**3.12 mW**	615 µW
C	42 µW	730 µW	

B2

1 1.34 mW	**2** 3.13 mW	**3** 3.4 mW
4 3.3 mW	**5** 3.26 mW	**6** 3.32 mW
7 2.82 mW	**8** 3.19 mW	**9** 3.08 mW

E3

	1	2	3
A	841 µW	4.05 mW	2.07 mW
B	**6.9 mW**	5.45 mW	2.95 mW
C	4.02 mW	5.25 mW	5.01 mW

B1

1 3.85 mW	**2** 5.7 mW	**3** 4.8 mW
4 4.89 mW	**5** 7.25 mW	**6** 7.4 mW
7 4.43 mW	**8** 7.3 mW	**9** 5.5 mW

E4

	1	2	3	4
A	1.9 mW	3.36 mW	3.5 mW	7 mW
B	307 µW	2.39 mW	5.02 mW	6.5 mW
C	230 µW	2.6 mW	**9 mW**	366 µW

C3

1 2.9 mW	**2** 4.5 mW	**3** 7.7 mW
4 8.9 mW	**5** 9.3 mW	**6** 9.1 mW
7 4.9 mW	**8** 2.2 mW	**9** 5.3 mW

E5

	1	2	3
A	2.72 mW	5.6 mW	2.06 mW
B	**9 mW**	5.6 mW	8.06 mW
C	8.2 mW	6.2 mW	2.3 mW

B1

1 6.9 mW	**2** 8.9 mW	**3** 2.8 mW
4 4.4 mW	**5** 9.33 mW	**6** 5.1 mW
7 6.12 mW	**8** 8.2 mW	**9** 4.9 mW

E6

	1	2	3
A	700 µW	5.5 mW	8.9 mW
B	2.06 mW	3.8 mW	13.84 mW
C	6.1 mW	**14 mW**	78 µW

C2

1 12.9 mW	**2** 9.5 mW	**3** 9.7 mW
4 14.17 mW	**5** 13.3 mW	**6** 10.2 mW
7 13.41 mW	**8** 12.37 mW	**9** 4.01 mW

Figure 4.11 shows the plot of maximum intensity obtained versus height of the elliptical mold. This trend helped us corroborate the results obtained by our setup and worked as reference data. The heights obtained for E1, E2 and E6 show a low standard variation. However, for E3, E4 and E5, the high variation is mainly due to the heterogeneity of heights along the surface.

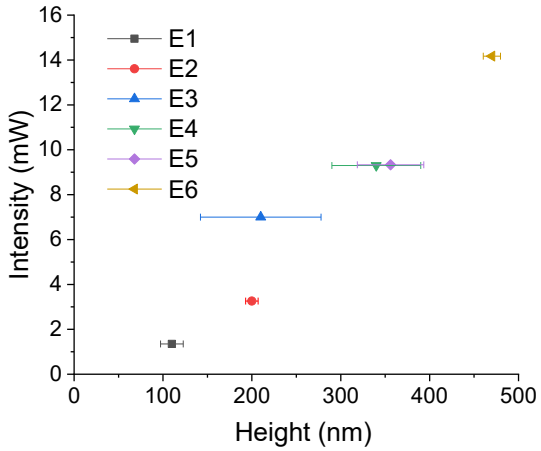

Figure 4.11. Intensity versus height of the maximum points of the PLA films with elliptical gratings

4.6 Degradation of PLA films with elliptical gratings

PLA films with elliptical gratings were used to observe the degradation curves obtained by the setup to know the influence of different geometry in the degradation rate. I immersed the PLA films with elliptical gratings in the optimum degradation environment obtained in section 4.2.

In Figure 4.12 (a), the 2D cross-section line profiles of the elliptical molds are presented to facilitate the comparison of the differences in heights. I can observe they possess different heights (from 110 to 470 nm), but the pitch varies from 1 µm ± 0.5 µm. The shape presented is a half ellipse excepting for E1 and E2, which presents a more sinusoidal profile rather than a half ellipse shape.

Figure 4.12 (b) presents the normalized intensity from the first-order diffraction beam versus time of the six different elliptical molds. These molds were studied under the optimum conditions of pH 8, 200 µg/mL of enzyme at 37°C. The degradation time takes up to 2 hours. E1 is the lowest in height according to the AFM image, and it does not present drastic intensity changes after the first 30 minutes. E2 and E3 present a decay during the first 30 minutes which is less abrupt that the one presented by E4 and E5. However, E6 is the one that present the most drastic change in the first minutes of the experiment, dropping its intensity up to 0.3 during the first 7 minutes, which leads to disappearance of the diffraction grating after around one hour and 30 minutes.

Figure 4.12 (c) presents the elliptical molds ordered in increasing intensity showing the trend of E1<E2<E3<E4<E5<E6. The trend agrees with the literature that mentions that intensity increases as height increases [80], [121]. In the same manner, the trend is maintained as E1<E2<E3<E4<E5<E6 for the degradation rate.

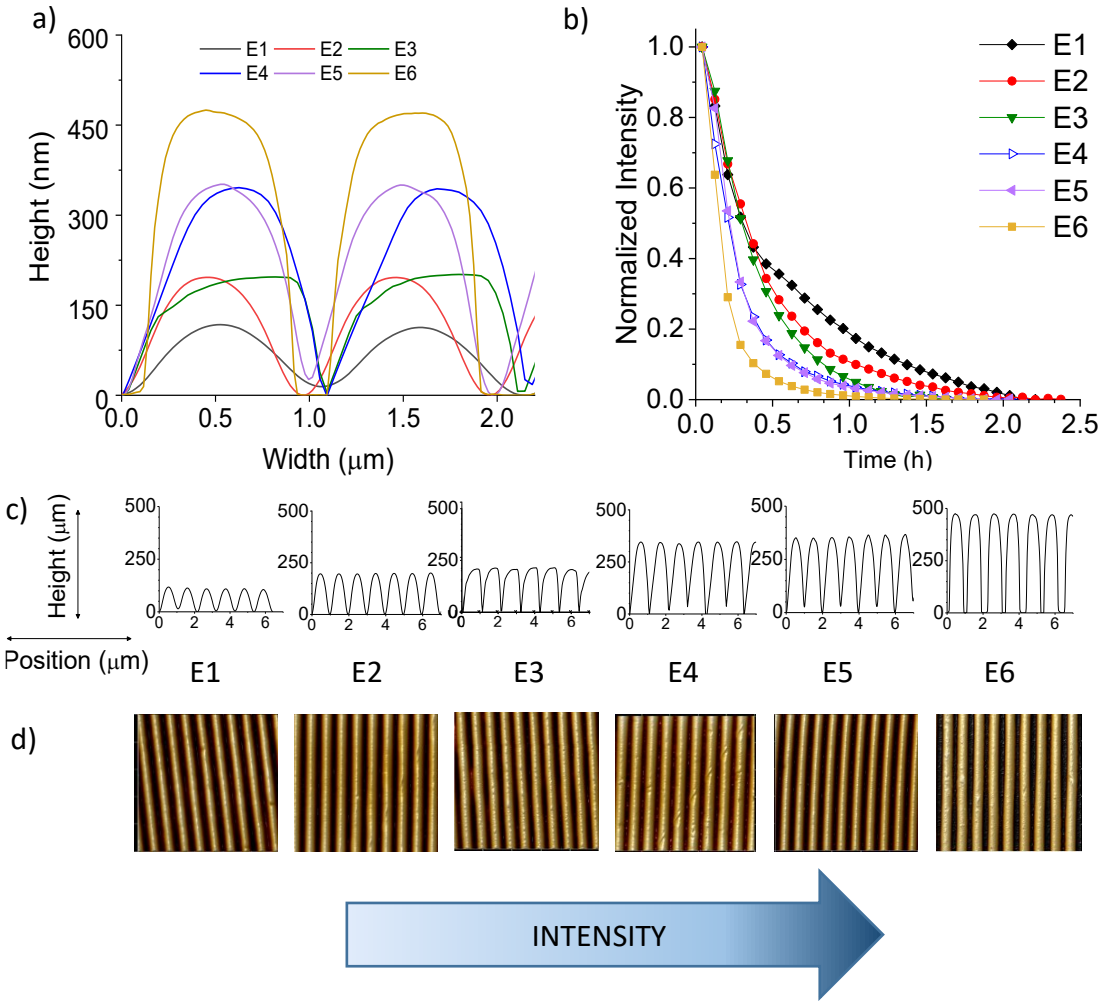

Figure 4.12. a) Profiles of the elliptical molds for comparison purposes b) evolution of the intensity of the first order diffraction for PLA gratings with elliptical features exposed to 200 ug/mL proteinase K solution at 37°C and pH 8, c) 2D individual cross-sectional profiles of the elliptical molds in increasing intensity, and d) surface morphology obtained by AFM for the elliptical molds.

In this section, elliptical molds were characterized by AFM, and the diffraction setup tracked their intensity evolution. The results suggest the importance of height as a factor that influences the diffraction intensity. In the case of surface eroding polymers, it is necessary to consider a shape factor since the surface area is related to the degradation rate [113]. As presented in the literature, height modifies the intensity of the diffracted beam [80], [121]. From these results, this method can study the influence of height in the degradation of PLA films with elliptical gratings

4.7 Simulation for PLA films with elliptical gratings

Theoretical graphs of intensity versus height were obtained by using theoretical data from OmniSim software. The geometry for these molds was presented in section 3.8 and corresponds to a half ellipse. For these simulations, the theoretical data was obtained to maximum height values exceeding the measured heights of the original gratings, 500 nm (E1 and E6) and 400 nm (E2, E3, E4 and E5), to be modified subsequently. To obtain this simulation data, it was indicated the height would decrease in a manner similar to the triangular gratings, while the other parameters like pitch (different for each mold), refractive index ($n_{water} = 1.33$ and $n_{PLA} = 1.5$), and substrate thickness ($10\ \mu m, n = 1.5$) were held constant. An individual simulation was done for each mold to obtain a theoretical intensity versus height plot.

The simulation data was modified for the specific heights of each mold. Therefore, the initial physical height was indicated, to obtain the theoretical intensity percentage corresponding to that height. The simulation data was renormalized to have the maximum physical intensity value measured as the maximum value. Subsequently, an initial etch rate was calculated using equation (3).

$$v = v_i - d\ (h_i - h_{sim}) \tag{3}$$

Where v_i is the initial etch rate, d is the rate decay constant, h_i is the initial height and h_{sim} is the simulated height. To obtain the initial etch rate and rate decay constant, first the theoretical data was interpolated to obtain the intensities corresponding to the experimental times. Subsequently, the difference between the theoretical interpolated intensity values and the experimental intensities was calculated. By using the least squares method, the minimum difference was obtained, calculating the initial etch rate and the rate decay constant that minimize this difference.

The measured data was fitted with the simulation data and the results are presented in Figure 4.13. In these figures, it is possible to observe how the simulations fit satisfactorily the measured intensities. For E1, the measured data presents some irregularities; this may be caused by the initial low height of this mold, which reduces the degradation timeframe and gives data closer to noise signal. For the rest of the molds, the simulation data showed slight differences around 30 minutes.

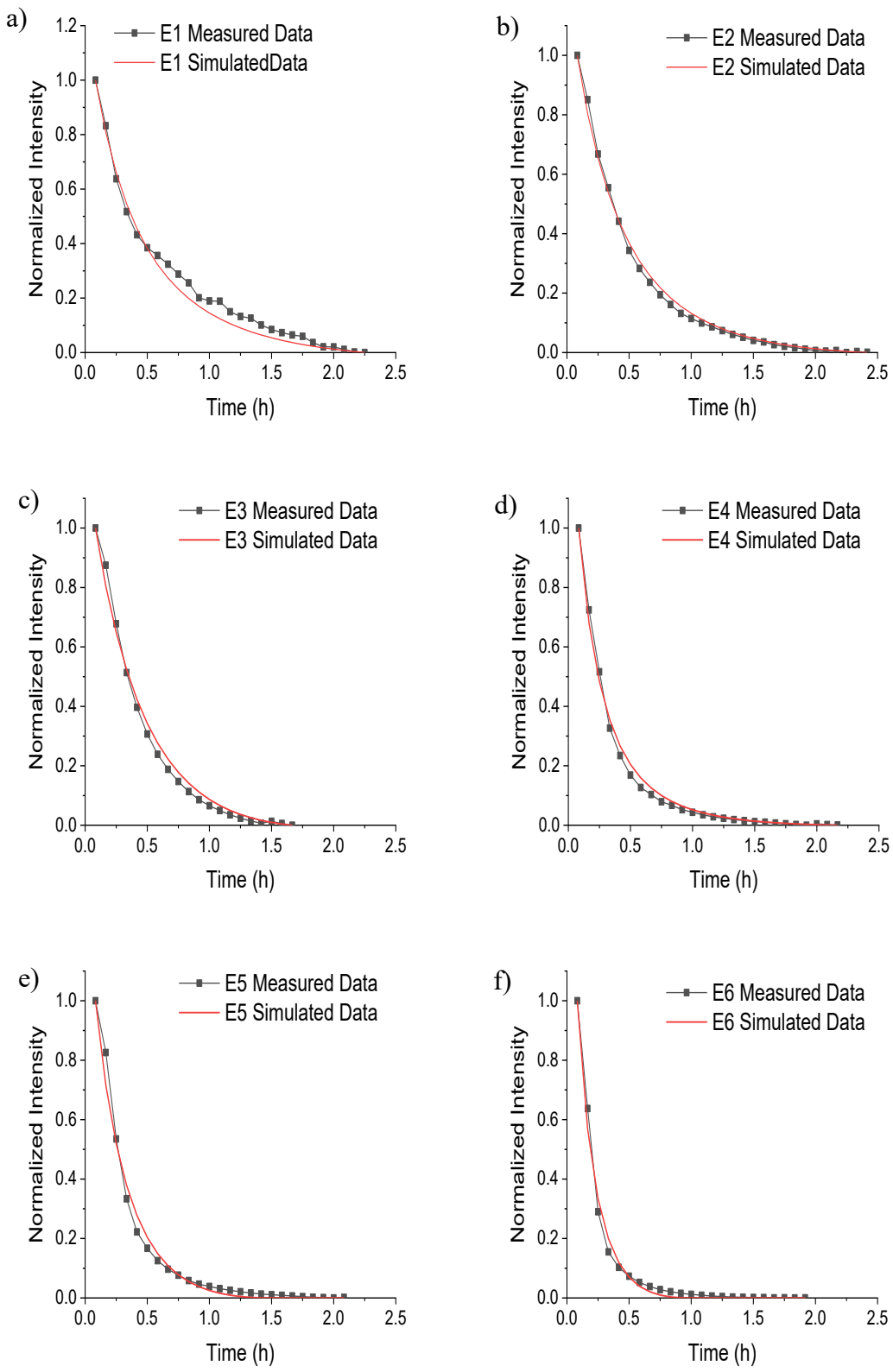

Figure 4.13. Normalized intensity versus time plots of the elliptical molds of measured data and simulated data

Table 4-4 shows the etch rates obtained. The trend demonstrated is E1<E2<E3<E4<E5<E6. These etch rates values increased as the height increased. This can be caused by a larger exposed area available to enzyme adsorption.

Table 4-4. Elliptical molds etch rates obtained

Mold	**Etch Rate (nm/min)**
E1	2.1
E2	4.3
E3	5.0
E4	11.9
E5	12.4
E6	28.08

In Chapter IV, PDMS intermediate molds were fabricated to produce PLA films by a solvent-casting method. The stability of PLA films was studied using the diffraction-based characterization method. This method could evaluate the changes in parameters like pH, enzyme concentration and temperature that were modified to obtain the optimum degradation conditions. AFM images of samples exposed to different times to the enzymatic solution at the optimum conditions; relate the decrease in intensity to the reduction in height. By linking intensity data to grating geometry, quantitative information could be obtained. Additionally, the shape effect on the etch rate was determined. Therefore, the results from this chapter provide information to understand PLA thin film degradation.

5. Conclusions and future direction

5.1 Conclusions

In this work, a diffraction-based degradation method previously introduced by our group was used to evaluate PLA thin film stability under different degradation environments. These conditions varied in pH, temperature, and concentration. Therefore, this study not only explored the stability of PLA thin films but also it was used to observe the effects of these parameters on the degradation rate. The experimental results were fitted using simulation data, and degradation etch rates were obtained. In addition, the impact of a different grating shape was investigated. The new shape data were also fitted to obtain etch rates. Thus, this method was able to provide information about polymer thin films in different conditions with different patterns on their surfaces.

Some of the most significant results include that PDMS molds were obtained from the master molds by a replica process. Using the PDMS molds, the PLA thin films were successfully patterned using a solvent-casting method. The proposed method was able to track the intensity of the diffracted beam subject to variations in temperature, pH, and enzyme concentration. By using triangular PLA thin films, it was shown that the higher temperatures experiment were the fastest during the first 30 minutes. However, the optimum degradation conditions correspond to 200 μg/mL, pH 8 at 37ºC, providing the fastest complete decay of intensity over time. PLA is a polymer that undergoes bulk degradation. However, the AFM images obtained at different degradation times more accurately related the decrease of intensity to surface degradation. These images helped to elucidate the possibility of the beam disappearance by swelling, and the change of degradation type is a significant sign of how the material properties change due to their dimensions.

Additionally, the simulation was able to provide an initial etch rate for these conditions of 8.5 nm/min. With prolonged immersion, a decrease in this etch rate was observed, meaning it was not constant, but a process that slows down as time passed. This result was fundamental to understanding PLA film enzymatic degradation, which is not well characterized by current methods.

Among the results achieved, the characterization method was able to track the influence of high temperatures showing high initial etch rates and enzyme deactivation after 1 hour. The

fact that a dim diffracted beam could still be discerned at the end of the four-hour experiment supports this interpretation. I also found that the degradation rate was not affected by refreshing the enzymatic solution, which provided information about the enzyme adsorption and the lack of binding sites. The measured degradation rate vs. pH trend agrees with the known behavior of the enzymes in their optimum conditions and at conditions outside their working range.

Although a triangular shape was used to find the optimum conditions, an elliptical shape was used to study the influence of shape on the degradation rate. During the second experimental stage, PLA films successfully embossed with elliptical gratings were exposed to the optimum parameters obtained. These molds presented different heights of the diffraction gratings. However, height and intensity were directly related. On the other hand, the etch rates for these molds were also obtained.

The simulation data presented in the current work helped to gain an insight into the enzymatic degradation of PLA films. The proposed method characterized PLA thin film stability in a simple manner without expensive equipment and exhaustive preparation. In addition, using theoretical data, it was possible to provide quantitative information about the initial etch rate in nm/min.

This diffraction-based method was able to relate the decrease in height with a decrease in intensity. It could also track the behavior of PLA films by matching simulated intensity profiles with experimental data. Therefore, in this work, a sensitive technique was developed to study polymer degradation.

5.2 Future directions

The work presented here maintained its focus on the application of a diffraction-based method to evaluate PLA film stability in the presence of proteinase K. However, it can be complemented in the future by the film's exposure to different degradation microorganisms. For instance, Tokiwa and Calabia observed that PLA could be degraded in the presence of *Amycolatopsis* (strain HT 32, 3118, KT-s-9, 41, and K104-1), *Bacillus brevis*, *Geobacillus thermocatenulatus*, *Cryptococcus* strain S-2, among others [49]. The results can be compared to know which microorganisms degrade PLA surfaces and under which parameters. Additionally, the degradation conditions for these different microorganisms can be varied to

study the influence of these changes in the degradation rate and the sensitivity of the microorganisms.

In the same manner, this method can also be used to explore the polymer thin film performance facing degradation conditions already proven for bulk PLA. Within these conditions, there exist PLA hydrolysis at 60ºC, 70ºC and 80ºC, as well as, hydrolysis with a pH range from 1 to 12 [122]. Equally, the experiment where the enzyme solution was changed can be modified by washing with 40% alcohol between the solution change since proteinase K has been shown to adsorb irreversibly in PLA films [123]. Therefore, this diffraction-based technique could help to build a database of PLA thin films exposed to different degradation environments improving the overall understanding of the stability of PLA thin films. This information can provide insight into the difference between bulk PLA degradation and thin-film degradation.

On the other hand, this technique can study PLA blends. There exist several alternatives for PLA plasticizers. However, it is necessary to focus on bio-plasticizers to maintain biodegradability. For instance, Li et al. have used polyethylene glycol (PEG) as a nontoxic, biodegradable, miscible plasticizer [124]. They also used epoxidized soybean oil, lactide and PLA oligomer [124]. Depending on the plasticizer, PLA chain mobility and properties such as ductility can increase [124]. However, it is necessary to study how the addition of these components affects its biodegradability (examining the addition in different quantities).

Regarding the studies with elliptical molds, supplementary research of their surfaces is needed. Additionally, the highest mold should be observed by AFM at different degradation times. The results from these experiments could be compared with the ones previously acquired. These images can help to track the degradation process and to corroborate the surface degradation presented in the triangular patterned films. These intensity versus time data could help to build a fitting model to support the etch rate values already obtained. To continue studying the shape effect, further geometries should be explored. Thin films could be patterned with different forms of different heights to evaluate this influence.

Moreover, the processing and the compounding method also influence PLA properties, and that effect can be studied with this technique. For example, the film fabrication method can be modified. It can be changed from a solvent-casting process to an imprinting technique. Instead of using PDMS molds as the mold to cast the liquid, it would be used as a stamp, as

shown by Bhadauriya et al. [125]. The resultant films would provide information about the effects of changes due to processing techniques (e.g. relaxation and constraints) in the degradation rates.

The biodegradability of PLA was studied because it is one of the most investigated biopolymers due to its characteristics [126]. Nevertheless, this work can be expanded by studying other biopolymers, which can potentially provide information about polymer thin film stability.

By considering the studies previously mentioned, this technique could help to ensure the integration of biopolymers in a variety of thin-film applications. In the same manner, the information of the behavior would contribute to the film's utilization, providing an alternative to fossil fuel polymers and preventing this excessive plastic waste production.

References

[1] C. Violatti, "Stone Age," *Ancient History Encyclopedia*, Jul-2014. [Online]. Available: https://www.ancient.eu/Stone_Age/. [Accessed: 01-Oct-2019].

[2] R. C. Thompson, S. H. Swan, C. J. Moore, and F. S. vom Saal, "Our plastic age," *Philos. Trans. R. Soc. B Biol. Sci.*, vol. 364, no. 1526, pp. 1973–1976, Jul. 2009, doi: 10.1098/rstb.2009.0054.

[3] J. Hopewell, R. Dvorak, and E. Kosior, "Plastics recycling: challenges and opportunities," *Phil Trans R Soc B*, vol. 364, no. 1526, pp. 2115–2126, Jul. 2009, doi: 10.1098/rstb.2008.0311.

[4] R. Geyer, J. R. Jambeck, and K. L. Law, "Production, use, and fate of all plastics ever made," *Sci. Adv.*, vol. 3, no. 7, p. e1700782, Jul. 2017, doi: 10.1126/sciadv.1700782.

[5] E. K. Liu, W. Q. He, and C. R. Yan, "`White revolution' to `white pollution': agricultural plastic film mulch in China," *Environ. Res. Lett.*, vol. 9, no. 9, p. 091001, Sep. 2014, doi: 10.1088/1748-9326/9/9/091001.

[6] L. T. Sin, A. R. Rahmat, and W. A. W. A. Rahman, Eds., "Overview of Polylactic acid," in *Polylactic Acid*, Oxford: William Andrew Publishing, 2013.

[7] J. M. Garcia and M. L. Robertson, "The future of plastics recycling," *Science*, vol. 358, no. 6365, pp. 870–872, Nov. 2017, doi: 10.1126/science.aaq0324.

[8] A. Banerjee, K. Chatterjee, and G. Madras, "Enzymatic degradation of polymers: a brief review," *Mater. Sci. Technol.*, vol. 30, no. 5, pp. 567–573, May 2014, doi: 10.1179/1743284713Y.0000000503.

[9] X. Ren, "Biodegradable plastics: a solution or a challenge?," *J. Clean. Prod.*, vol. 11, no. 1, pp. 27–40, Feb. 2003, doi: 10.1016/S0959-6526(02)00020-3.

[10] A. L. Andrady, "The plastic in microplastics: A review," *Mar. Pollut. Bull.*, vol. 119, no. 1, pp. 12–22, Jun. 2017, doi: 10.1016/j.marpolbul.2017.01.082.

[11] C. Wilcox, E. Van Sebille, and B. D. Hardesty, "Threat of plastic pollution to seabirds is global, pervasive, and increasing," *Proc. Natl. Acad. Sci.*, vol. 112, no. 38, pp. 11899–11904, Sep. 2015, doi: 10.1073/pnas.1502108112.

[12] F. Signori, M.-B. Coltelli, and S. Bronco, "Thermal degradation of poly(lactic acid) (PLA) and poly(butylene adipate-co-terephthalate) (PBAT) and their blends upon melt processing," *Polym. Degrad. Stab.*, vol. 94, no. 1, pp. 74–82, Jan. 2009, doi: 10.1016/j.polymdegradstab.2008.10.004.

[13] J. Ren, "Standard and Test Methods," in *Biodegradable Poly(Lactic Acid): Synthesis, Modification, Processing and Applications*, J. Ren, Ed. Berlin, Heidelberg: Springer, 2010, pp. 273–296.

[14] P. Anbukarasu, D. I. Martínez-Tobón, D. Sauvageau, and A. L. Elias, "A diffraction-based degradation sensor for polymer thin films," *Polym. Degrad. Stab.*, vol. 142, pp. 102–110, Aug. 2017, doi: 10.1016/j.polymdegradstab.2017.05.020.

[15] B. Stern, C. Heron, L. Corr, M. Serpico, and J. Bourriau, "Compositional Variations in Aged and Heated Pistacia Resin Found in Late Bronze Age Canaanite Amphorae and Bowls from Amarna, Egypt," *Archaeometry*, vol. 45, no. 3, pp. 457–469, 2003, doi: 10.1111/1475-4754.00121.

[16] L. Parker, "We made plastic. We depend on ti, Now we're drowning in it," *National Geographic*, 16-May-2018.

[17] D. Allen *et al.*, "Sustainable Materials Management," United States Environmental Protection Agency, 2009.
[18] M. A. Elsawy, K.-H. Kim, J.-W. Park, and A. Deep, "Hydrolytic degradation of polylactic acid (PLA) and its composites," *Renew. Sustain. Energy Rev.*, vol. 79, pp. 1346–1352, Nov. 2017, doi: 10.1016/j.rser.2017.05.143.
[19] C. M. Rochman *et al.*, "Anthropogenic debris in seafood: Plastic debris and fibers from textiles in fish and bivalves sold for human consumption," *Sci. Rep.*, vol. 5, no. 1, p. 14340, Nov. 2015, doi: 10.1038/srep14340.
[20] M. Shen *et al.*, "Recent advances in toxicological research of nanoplastics in the environment: A review," *Environ. Pollut.*, vol. 252, pp. 511–521, Sep. 2019, doi: 10.1016/j.envpol.2019.05.102.
[21] R. Rebelo, M. Fernandes, and R. Fangueiro, "Biopolymers in Medical Implants: A Brief Review," *Procedia Eng.*, vol. 200, pp. 236–243, 2017, doi: 10.1016/j.proeng.2017.07.034.
[22] Y. Tokiwa, B. P. Calabia, C. U. Ugwu, and S. Aiba, "Biodegradability of Plastics," *Int. J. Mol. Sci.*, vol. 10, no. 9, pp. 3722–3742, Aug. 2009, doi: 10.3390/ijms10093722.
[23] R. A. Gross, "Biodegradable Polymers for the Environment," *Science*, vol. 297, no. 5582, pp. 803–807, Aug. 2002, doi: 10.1126/science.297.5582.803.
[24] K. Madhavan Nampoothiri, N. R. Nair, and R. P. John, "An overview of the recent developments in polylactide (PLA) research," *Bioresour. Technol.*, vol. 101, no. 22, pp. 8493–8501, Nov. 2010, doi: 10.1016/j.biortech.2010.05.092.
[25] E. Castro-Aguirre, F. Iñiguez-Franco, H. Samsudin, X. Fang, and R. Auras, "Poly(lactic acid)—Mass production, processing, industrial applications, and end of life," *Adv. Drug Deliv. Rev.*, vol. 107, pp. 333–366, Dec. 2016, doi: 10.1016/j.addr.2016.03.010.
[26] R. Wool and X. S. Sun, *Bio-Based Polymers and Composites*, 1st ed. United States: Elsevier, 2005.
[27] H. Nakajima, P. Dijkstra, and K. Loos, "The Recent Developments in Biobased Polymers toward General and Engineering Applications: Polymers that are Upgraded from Biodegradable Polymers, Analogous to Petroleum-Derived Polymers, and Newly Developed," *Polymers*, vol. 9, no. 10, p. 523, Oct. 2017, doi: 10.3390/polym9100523.
[28] T. Iwata, H. Abe, and Y. Kikkawa, "Enzymatic Degradation," in *Poly(Lactic Acid)*, Wiley-Blackwell, 2010, pp. 383–399.
[29] J. R. Wagner, Ed., *Multilayer Flexible Packaging*, 2nd ed. Elsevier, 2016.
[30] L. N. Woodard and M. A. Grunlan, "Hydrolytic Degradation and Erosion of Polyester Biomaterials," *ACS Macro Lett.*, vol. 7, no. 8, pp. 976–982, Aug. 2018, doi: 10.1021/acsmacrolett.8b00424.
[31] R. Auras, B. Harte, and S. Selke, "An Overview of Polylactides as Packaging Materials," *Macromol Biosci*, vol. 4, no. 9, pp. 835–864, Sep. 2004, doi: 10.1002/mabi.200400043.
[32] R. Auras, L.-T. Lim, S. E. M. Selke, and T. Hideto, "Poly(lactic acid): Synthesis, Structures, Properties, Processing, and Applications," in *Poly(Lactic Acid)*, John Wiley & Sons, Ltd, 2010.
[33] K. Masutani and Y. Kimura, "Chapter 1:PLA Synthesis. From the Monomer to the Polymer," in *Poly(lactic acid) Science and Technology*, 2014, pp. 1–36.
[34] Y. Tokiwa and A. Jarerat, "Biodegradation of poly(l-lactide)," *Biotechnol. Lett.*, vol. 26, no. 10, pp. 771–777, May 2004, doi: 10.1023/B:BILE.0000025927.31028.e3.

[35] Y. Pan, M. Farmahini-Farahani, P. O'Hearn, H. Xiao, and H. Ocampo, "An overview of bio-based polymers for packaging materials," *J. Bioresour. Bioprod.*, vol. Vol 1, pp. 106-113 Pages, Jul. 2016, doi: 10.21967/jbb.v1i3.49.
[36] R. P. Babu, K. O'Connor, and R. Seeram, "Current progress on bio-based polymers and their future trends," *Prog. Biomater.*, vol. 2, no. 1, p. 8, Mar. 2013, doi: 10.1186/2194-0517-2-8.
[37] J. Esmaeilzadeh, S. Hesaraki, S. M.-M. Hadavi, M. Esfandeh, and M. H. Ebrahimzadeh, "Microstructure and mechanical properties of biodegradable poly (D/L) lactic acid/polycaprolactone blends processed from the solvent-evaporation technique," *Mater. Sci. Eng. C Mater. Biol. Appl.*, vol. 71, pp. 807–819, Feb. 2017, doi: 10.1016/j.msec.2016.10.070.
[38] S. Farah, D. G. Anderson, and R. Langer, "Physical and mechanical properties of PLA, and their functions in widespread applications — A comprehensive review," *Adv. Drug Deliv. Rev.*, vol. 107, pp. 367–392, Dec. 2016, doi: 10.1016/j.addr.2016.06.012.
[39] Y. Luo, Z. Lin, and G. Guo, "Biodegradation Assessment of Poly (Lactic Acid) Filled with Functionalized Titania Nanoparticles (PLA/TiO2) under Compost Conditions," *Nanoscale Res. Lett.*, vol. 14, no. 1, p. 56, Feb. 2019, doi: 10.1186/s11671-019-2891-4.
[40] H. Nishida, "Thermal Degradation," in *Poly(Lactic Acid)*, R. Auras, L.-T. Lim, S. E. M. Selke, and H. Tsuji, Eds. Hoboken, NJ, USA: John Wiley & Sons, Inc., 2010, pp. 401–412.
[41] N. Kameno, S. Yamada, T. Amimoto, K. Amimoto, H. Ikeda, and N. Koga, "Thermal degradation of poly(lactic acid) oligomer: Reaction mechanism and multistep kinetic behavior," *Polym. Degrad. Stab.*, vol. 134, pp. 284–295, Dec. 2016, doi: 10.1016/j.polymdegradstab.2016.10.018.
[42] W. L. Hawkins, Ed., *Polymer Degradation*, vol. 8. Berlin, Heidelberg, 1984.
[43] J. Lunt, "Large-scale production, properties and commercial applications of polylactic acid polymers," *Polym. Degrad. Stab.*, vol. 59, no. 1, pp. 145–152, Jan. 1998, doi: 10.1016/S0141-3910(97)00148-1.
[44] A. C. Vieira, A. T. Marques, R. M. Guedes, and V. Tita, "Material model proposal for biodegradable materials," *Procedia Eng.*, vol. 10, pp. 1597–1602, 2011, doi: 10.1016/j.proeng.2011.04.267.
[45] D. F. Williams, "Enzymic Hydrolysis of Polylactic Acid," *Eng. Med.*, vol. 10, no. 1, pp. 5–7, Jan. 1981, doi: 10.1243/EMED_JOUR_1981_010_004_02.
[46] S. H. Lee, I. Y. Kim, and W. S. Song, "Biodegradation of polylactic acid (PLA) fibers using different enzymes," *Macromol. Res.*, vol. 22, no. 6, pp. 657–663, Jun. 2014, doi: 10.1007/s13233-014-2107-9.
[47] S. H. Lee and W. S. Song, "Modification of polylactic acid fabric by two lipolytic enzyme hydrolysis," *Text. Res. J.*, vol. 83, no. 3, pp. 229–237, Feb. 2013, doi: 10.1177/0040517512458345.
[48] M. M. Burrell, Ed., *Enzymes of molecular biology*. Totowa, N.J: Humana Press, 1993.
[49] Y. Tokiwa and B. P. Calabia, "Biodegradability and biodegradation of poly(lactide)," *Appl. Microbiol. Biotechnol.*, vol. 72, no. 2, pp. 244–251, Sep. 2006, doi: 10.1007/s00253-006-0488-1.
[50] H. Tsuji and H. Muramatsu, "Blends of aliphatic polyesters: V non-enzymatic and enzymatic hydrolysis of blends from hydrophobic poly(l-lactide) and hydrophilic

poly(vinyl alcohol)," *Polym. Degrad. Stab.*, vol. 71, no. 3, pp. 403–413, Jan. 2001, doi: 10.1016/S0141-3910(00)00192-0.
[51] A. A. Shah, F. Hasan, A. Hameed, and S. Ahmed, "Biological degradation of plastics: A comprehensive review," *Biotechnol. Adv.*, vol. 26, no. 3, pp. 246–265, May 2008, doi: 10.1016/j.biotechadv.2007.12.005.
[52] J.-H. Huang and V. M. Ugaz, "A membraneless continuous-flow filter for high-throughput separation and enrichment of particles and cells," in *2010 AIChE Annual Meeting*, Salt Lake City, 2010, p. 3.
[53] A. R. Gomes and T. A. P. Rocha-Santos, "Bioassays: Enzyme Assays," in *Encyclopedia of Analytical Science (Third Edition)*, P. Worsfold, C. Poole, A. Townshend, and M. Miró, Eds. Oxford: Academic Press, 2019, pp. 271–277.
[54] "Effects of pH: Introduction to Enzymes." [Online]. Available: http://www.worthington-biochem.com/introBiochem/effectspH.html. [Accessed: 11-Oct-2019].
[55] R.-J. Mueller, "Biological degradation of synthetic polyesters—Enzymes as potential catalysts for polyester recycling," *Process Biochem.*, vol. 41, no. 10, pp. 2124–2128, Oct. 2006, doi: 10.1016/j.procbio.2006.05.018.
[56] H. Pranamuda, Y. Tokiwa, and H. Tanaka, "Polylactide Degradation by an Amycolatopsis sp," *Appl. Environ. Microbiol.*, vol. 63, no. 4, pp. 1637–1640, Apr. 1997.
[57] F. Kawai, "Breakdown of plastics and polymers by microorganisms," in *Microbial and Eznymatic Bioproducts*, vol. 52, Berlin, Heidelberg: Springer Berlin Heidelberg, 1995, pp. 151–194.
[58] B. Tyler, D. Gullotti, A. Mangraviti, T. Utsuki, and H. Brem, "Polylactic acid (PLA) controlled delivery carriers for biomedical applications," *Adv. Drug Deliv. Rev.*, vol. 107, pp. 163–175, Dec. 2016, doi: 10.1016/j.addr.2016.06.018.
[59] M. Murariu and P. Dubois, "PLA composites: From production to properties," *Adv. Drug Deliv. Rev.*, vol. 107, pp. 17–46, Dec. 2016, doi: 10.1016/j.addr.2016.04.003.
[60] C. Liu, Y. Jia, and A. He, "Preparation of Higher Molecular Weight Poly (L-lactic Acid) by Chain Extension," *Int J Polym Sci*, vol. 2013, p. 6, 2013, doi: 10.1155/2013/315917.
[61] M. Jamshidian, E. A. Tehrany, M. Imran, M. Jacquot, and S. Desobry, "Poly-Lactic Acid: Production, Applications, Nanocomposites, and Release Studies," *Compr. Rev. Food Sci. Food Saf.*, vol. 9, no. 5, pp. 552–571, 2010, doi: 10.1111/j.1541-4337.2010.00126.x.
[62] K. P. Gritsenko and A. M. Krasovsky, "Thin-Film Deposition of Polymers by Vacuum Degradation," *Chem. Rev.*, vol. 103, no. 9, pp. 3607–3650, Sep. 2003, doi: 10.1021/cr010449q.
[63] American Plastics Council, "Understanding Plastic Film: Its Uses, Benefits and Waste Management Options.," 1997. [Online]. Available: https://plastics.americanchemistry.com/Understanding-Plastic-Film/.
[64] S. Li and S. McCarthy, "Further investigations on the hydrolytic degradation of poly (DL-lactide)," *Biomaterials*, vol. 20, no. 1, pp. 35–44, Jan. 1999, doi: 10.1016/S0142-9612(97)00226-3.
[65] C. Sumner, S. Krause, A. Sabot, K. Turner, and C. J. McNeil, "Biosensor based on enzyme-catalysed degradation of thin polymer films," *Biosens. Bioelectron.*, vol. 16, no. 9, pp. 709–714, Dec. 2001, doi: 10.1016/S0956-5663(01)00210-X.
[66] B. Schyrr, S. Boder-Pasche, R. Ischer, R. Smajda, and G. Voirin, "Fiber-optic protease sensor based on the degradation of thin gelatin films," *Sens. Bio-Sens. Res.*, vol. 3, pp. 65–73, Mar. 2015, doi: 10.1016/j.sbsr.2014.12.004.

[67] Y.-X. Liu and E.-Q. Chen, "Polymer crystallization of ultrathin films on solid substrates," *Coord. Chem. Rev.*, vol. 254, no. 9–10, pp. 1011–1037, May 2010, doi: 10.1016/j.ccr.2010.02.017.
[68] P. Xu, T. Xu, H. Yu, and X. Li, "Resonant-Gravimetric Identification of Competitive Adsorption of Environmental Molecules," *Anal. Chem.*, vol. 89, no. 13, pp. 7031–7037, Jul. 2017, doi: 10.1021/acs.analchem.7b00723.
[69] K. A. Marx, "Quartz Crystal Microbalance: A Useful Tool for Studying Thin Polymer Films and Complex Biomolecular Systems at the Solution−Surface Interface," *Biomacromolecules*, vol. 4, no. 5, pp. 1099–1120, Sep. 2003, doi: 10.1021/bm020116i.
[70] M. D. Millan, J. Locklin, T. Fulghum, A. Baba, and R. C. Advincula, "Polymer thin film photodegradation and photochemical crosslinking: FT-IR imaging, evanescent waveguide spectroscopy, and QCM investigations," *Polymer*, vol. 46, no. 15, pp. 5556–5568, Jul. 2005, doi: 10.1016/j.polymer.2005.05.050.
[71] R. Bhargava, S.-Q. Wang, and J. L. Koenig, "FTIR Imaging Studies of a New Two-Step Process To Produce Polymer Dispersed Liquid Crystals," *Macromolecules*, vol. 32, no. 8, pp. 2748–2760, Apr. 1999, doi: 10.1021/ma981542s.
[72] C.-S. Wu, *Handbook Of Size Exclusion Chromatography And Related Techniques: Revised And Expanded*, 2nd ed., vol. 91. CRC Press, 2003.
[73] P. Anbukarasu, D. Sauvageau, and A. L. Elias, "Enzymatic degradation of dimensionally constrained polyhydroxybutyrate films," *Phys. Chem. Chem. Phys.*, vol. 19, no. 44, pp. 30021–30030, Nov. 2017, doi: 10.1039/C7CP05133F.
[74] E. Hecht, *Optics*, 5th ed. England: Pearson Education Limited, 2017.
[76] E. G. Loewen and E. Popov, *Diffraction Gratings and Applications*. CRC Press, 1997.
[76] C. Palmer and E. Loewen, *Diffraction Grating Handbook*, 6th ed. Newport Corporation, 2005.
[77] "Definitive Guide to Diffraction Grating | Dynasil Corporation." [Online]. Available: https://www.dynasil.com/optical-materials/buyers-guide-to-selecting-a-diffraction-grating/. [Accessed: 10-Oct-2019].
[78] "Diffraction Gratings - Shimadzu," 09-Feb-2018. [Online]. Available: https://www.shimadzu.com/opt/guide/diffraction/index.html. [Accessed: 15-Dec-2019].
[79] "Diffraction Efficiency - Plymouth Grating Laboratory." [Online]. Available: https://www.plymouthgrating.com/guidance/technical-notes/fundamentals/diffraction-efficiency/. [Accessed: 28-Jul-2019].
[80] D. C. O'Shea, T. J. Suleski, A. D. Kathman, and D. W. Prather, *Diffractive Optics: Design, Fabrication, and Test*. SPIE Press, 2004.
[81] N. Bonod and J. Neauport, "Diffraction gratings: from principles to applications in high-intensity lasers," *Adv. Opt. Photonics*, vol. 8, no. 1, p. 156, Mar. 2016, doi: 10.1364/AOP.8.000156.
[82] C.-L. Chang, G. Acharya, and C. A. Savran, "In situ assembled diffraction grating for biomolecular detection," *Appl. Phys. Lett.*, vol. 90, no. 23, p. 233901, Jun. 2007, doi: 10.1063/1.2746409.
[83] G. Ye and X. Wang, "Glucose sensing through diffraction grating of hydrogel bearing phenylboronic acid groups," *Biosens. Bioelectron.*, vol. 26, no. 2, pp. 772–777, Oct. 2010, doi: 10.1016/j.bios.2010.06.029.

[84] P. T. Fiori and M. F. Paige, “Detection of enzymatic activity by means of a diffraction-based biosensor,” *Anal. Bioanal. Chem.*, vol. 380, no. 2, pp. 339–342, Sep. 2004, doi: 10.1007/s00216-004-2741-8.
[85] J. B. Goh, R. W. Loo, and M. C. Goh, “Label-free monitoring of multiple biomolecular binding interactions in real-time with diffraction-based sensing,” *Sens. Actuators B Chem.*, vol. 106, no. 1, pp. 243–248, Apr. 2005, doi: 10.1016/j.snb.2004.08.003.
[86] Y. G. Tsay *et al.*, “Optical biosensor assay (OBA).,” *Clin. Chem.*, vol. 37, no. 9, pp. 1502–1505, Sep. 1991.
[87] F. Morhard, J. Pipper, R. Dahint, and M. Grunze, “Immobilization of antibodies in micropatterns for cell detection by optical diffraction,” *Sens. Actuators B Chem.*, vol. 70, no. 1, pp. 232–242, Nov. 2000, doi: 10.1016/S0925-4005(00)00574-8.
[88] Y. Fang, A. M. Ferrie, N. H. Fontaine, J. Mauro, and J. Balakrishnan, “Resonant Waveguide Grating Biosensor for Living Cell Sensing,” *Biophys. J.*, vol. 91, no. 5, pp. 1925–1940, Sep. 2006, doi: 10.1529/biophysj.105.077818.
[89] R. C. Bailey, J.-M. Nam, C. A. Mirkin, and J. T. Hupp, “Real-Time Multicolor DNA Detection with Chemoresponsive Diffraction Gratings and Nanoparticle Probes,” *J. Am. Chem. Soc.*, vol. 125, no. 44, pp. 13541–13547, Nov. 2003, doi: 10.1021/ja035479k.
[90] L. Peng, M. M. Varma, F. E. Regnier, and D. D. Nolte, “Adaptive optical biocompact disk for molecular recognition,” *Appl. Phys. Lett.*, vol. 86, no. 18, p. 183902, Apr. 2005, doi: 10.1063/1.1915511.
[91] H. Zhu, X. Jing, L. Chen, and Y. Tian, “Enhancement of antireflection characteristic of resonant sinusoidal grating,” *Opt. Commun.*, vol. 357, pp. 78–85, Dec. 2015, doi: 10.1016/j.optcom.2015.08.085.
[92] “Photonics Software with FDTD Engine for Optical Simulations – OmniSim: Applications Overview.” [Online]. Available: https://www.photond.com/products/omnisim/omnisim_applications_00.htm. [Accessed: 24-Sep-2019].
[93] S. Ebnesajjad, *Handbook of Biopolymers and Biodegradable Plastics: Properties, Processing and Applications*. United States: William Andrew, 2012.
[94] D. Z. Bucci, L. B. B. Tavares, and I. Sell, “PHB packaging for the storage of food products,” *Polym. Test.*, vol. 24, no. 5, pp. 564–571, Aug. 2005, doi: 10.1016/j.polymertesting.2005.02.008.
[95] S. Natarajan, D. A. Chang-Yen, and B. K. Gale, “Large-area, high-aspect-ratio SU-8 molds for the fabrication of PDMS microfluidic devices,” *J Micromech Microeng*, vol. 18, no. 4, p. 045021, Apr. 2008, doi: 10.1088/0960-1317/18/4/045021.
[96] “OmniSim and CrystalWave,” United Kingdom: Photon Design, 2018.
[97] M. Ayre, T. J. Karle, L. Wu, T. Davies, and T. F. Krauss, “Experimental Verification of Numerically Optimized Optimized Photonic Crystal Injector, Y-Splitter, and Bend,” *IEEE J Sel Area Comm*, vol. 23, no. 7, pp. 1390–1395, Jul. 2005, doi: 10.1109/JSAC.2005.851169.
[98] J. H. Kang, Y. Chang Kim, and J.-K. Park, “Analysis of pressure-driven air bubble elimination in a microfluidic device,” *Lab. Chip*, vol. 8, no. 1, pp. 176–178, 2008, doi: 10.1039/B712672G.
[99] S.-W. Kang, “Application of Soft Lithography for Nano Functional Devices,” in *Lithography*, M. Wang, Ed. 2010, p. 656.

[100] B. K. Gale *et al.*, "A Review of Current Methods in Microfluidic Device Fabrication and Future Commercialization Prospects," *Inventions*, vol. 3, no. 3, p. 60, Sep. 2018, doi: 10.3390/inventions3030060.
[101] K. Yamashita, Y. Kikkawa, K. Kurokawa, and Y. Doi, "Enzymatic Degradation of Poly(L -lactide) Film by Proteinase K: Quartz Crystal Microbalance and Atomic Force Microscopy Study," *Biomacromolecules*, vol. 6, no. 2, pp. 850–857, Mar. 2005, doi: 10.1021/bm049395v.
[102] P. K. Robinson, "Enzymes: principles and biotechnological applications," *Essays Biochem.*, vol. 59, pp. 1–41, Nov. 2015, doi: 10.1042/bse0590001.
[103] H. Bisswanger, "Enzyme assays," *Perspect. Sci.*, vol. 1, no. 1, pp. 41–55, May 2014, doi: 10.1016/j.pisc.2014.02.005.
[104] W. Ebeling, N. Hennrich, M. Klockow, H. Metz, H. D. Orth, and H. Lang, "Proteinase K from Tritirachium album Limber," *Eur. J. Biochem.*, vol. 47, no. 1, pp. 91–97, 1974, doi: 10.1111/j.1432-1033.1974.tb03671.x.
[105] W. Saenger, "Proteinase K," in *Handbook of Proteolytic Enzymes*, 3rd ed., vol. 2, Elsevier, 2013, pp. 3240–3242.
[106] M. S. Reeve, S. P. McCarthy, M. J. Downey, and R. A. Gross, "Polylactide stereochemistry: effect on enzymic degradability," *Macromolecules*, vol. 27, no. 3, pp. 825–831, Jan. 1994, doi: 10.1021/ma00081a030.
[107] H. Cai, V. Dave, R. A. Gross, and S. P. McCarthy, "Effects of physical aging, crystallinity, and orientation on the enzymatic degradation of poly(lactic acid)," *J. Polym. Sci. Part B Polym. Phys.*, vol. 34, no. 16, pp. 2701–2708, 1996, doi: 10.1002/(SICI)1099-0488(19961130)34:16<2701::AID-POLB2>3.0.CO;2-S.
[108] S. H. Lee and W. S. Song, "Enzymatic Hydrolysis of Polylactic Acid Fiber," *Appl. Biochem. Biotechnol.*, vol. 164, no. 1, pp. 89–102, May 2011, doi: 10.1007/s12010-010-9117-7.
[109] C. R. Rabin and S. J. Siegel, "Delivery Systems and Dosing for Antipsychotics," in *Current Antipsychotics*, G. Gross and M. A. Geyer, Eds. Berlin, Heidelberg: Springer, 2012, pp. 267–298.
[110] H. Azevedo and R. Reis, "Understanding the Enzymatic Degradation of Biodegradable Polymers and Strategies to Control Their Degradation Rate," in *Biodegradable Systems in Tissue Engineering and Regenerative Medicine*, R. Reis and J. San Román, Eds. CRC Press, 2004.
[111] T. Iwata and Y. Doi, "Morphology and Enzymatic Degradation of Poly(l-lactic acid) Single Crystals," *Macromolecules*, vol. 31, no. 8, pp. 2461–2467, Apr. 1998, doi: 10.1021/ma980008h.
[112] F. von Burkersroda, L. Schedl, and A. Göpferich, "Why degradable polymers undergo surface erosion or bulk erosion," *Biomaterials*, vol. 23, no. 21, pp. 4221–4231, Nov. 2002, doi: 10.1016/S0142-9612(02)00170-9.
[113] I. Grizzi, H. Garreau, S. Li, and M. Vert, "Hydrolytic degradation of devices based on poly[m-lactic acid) size- dependence," vol. 16, no. 4, p. 7, 1995.
[114] D. Garlotta, "A Literature Review of Poly(Lactic Acid)," *J. Polym. Environ.*, vol. 9, no. 2, pp. 63–84, 2001, doi: 10.1023/A:1020200822435.
[115] S. Lyu and D. Untereker, "Degradability of Polymers for Implantable Biomedical Devices," *Int. J. Mol. Sci.*, vol. 10, no. 9, pp. 4033–4065, Sep. 2009, doi: 10.3390/ijms10094033.

[116] C. Bastioli and Rapra Technology Limited, *Handbook of Biodegradable Polymers*. Shawbury, Shrewsbury, Shropshire, U.K.: Rapra Technology Ltd, 2005.
[117] A. Göpferich, "Mechanisms of polymer degradation and erosion," *Biomaterials*, vol. 17, no. 2, pp. 103–114, Jan. 1996, doi: 10.1016/0142-9612(96)85755-3.
[118] R. K. Scopes, "Enzyme Activity and Assays," in *eLS*, American Cancer Society, 2002.
[119] X. Han, J. Pan, F. Buchanan, N. Weir, and D. Farrar, "Analysis of degradation data of poly(l-lactide–co-l,d-lactide) and poly(l-lactide) obtained at elevated and physiological temperatures using mathematical models," *Acta Biomater.*, vol. 6, no. 10, pp. 3882–3889, Oct. 2010, doi: 10.1016/j.actbio.2010.05.015.
[120] J. W. Kamande, Y. Wang, and A. M. Taylor, "Cloning SU8 silicon masters using epoxy resins to increase feature replicability and production for cell culture devices," *Biomicrofluidics*, vol. 9, no. 3, p. 036502, May 2015, doi: 10.1063/1.4922962.
[121] R. Magnusson and T. K. Gaylord, "Diffraction efficiencies of thin phase gratings with arbitrary grating shape," *JOSA*, vol. 68, no. 6, pp. 806–809, Jun. 1978, doi: 10.1364/JOSA.68.000806.
[122] E. J. Rodriguez, B. Marcos, and M. A. Huneault, "Hydrolysis of polylactide in aqueous media," *J. Appl. Polym. Sci.*, vol. 133, no. 44, Nov. 2016, doi: 10.1002/app.44152.
[123] Z. Zhao *et al.*, "Relationship between Enzyme Adsorption and Enzyme-Catalyzed Degradation of Polylactides," *Macromol. Biosci.*, vol. 8, no. 1, pp. 25–31, 2008, doi: 10.1002/mabi.200700180.
[124] D. Li *et al.*, "Preparation of plasticized poly (lactic acid) and its influence on the properties of composite materials," *PLoS ONE*, vol. 13, no. 3, Mar. 2018, doi: 10.1371/journal.pone.0193520.
[125] S. Bhadauriya *et al.*, "Tuning the Relaxation of Nanopatterned Polymer Films with Polymer-Grafted Nanoparticles: Observation of Entropy–Enthalpy Compensation," *Nano Lett.*, vol. 18, no. 12, pp. 7441–7447, Dec. 2018, doi: 10.1021/acs.nanolett.8b02514.
[126] A. Jimenez, M. Peltzer, and R. Ruseckaite, Eds., *Poly(lactic acid) Science and Technology: Processing, Properties, Additives and Applications*. Royal Society of Chemistry, 2014.

Appendices

Appendix A: Additional Results

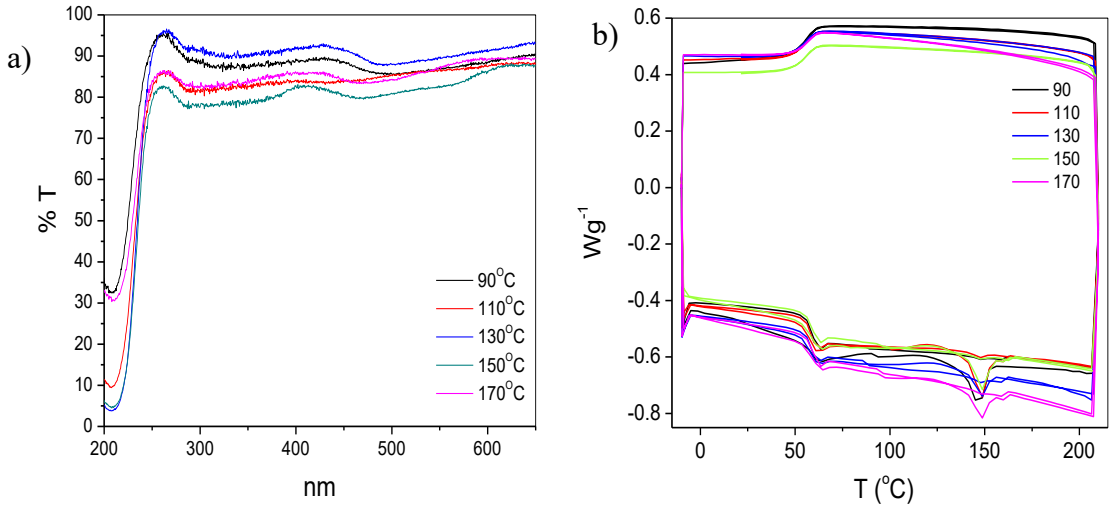

Figure A-1: Characterization of PLA film casted at different temperatures a)UV-vis and b) DSC of PLA films

Table A-1: DSC information from PLA films casted at different temperatures

	Sample	Melting T	T_G (ºC)		ΔH_M	Cristallinity
		(ºC)	Onset 1	Onset 2	(J/G)	%
1	90ºC	137.3	57.2	56.29	10.3	11.08
2	110ºC	141.88	53.68	55.48	10.24	11.01
3	130ºC	143.31	54.67	56.47	3.87	4.16
4	150ºC	142.6	54.04	56.72	8.37	9.00
5	170ºC	142.49	54.26	57.22	7.24	7.78

Appendix B: Permissions to Reproduce

- Permission to reproduce Table 2-1, which was published by Moataz A. Elsawy in "Hydrolytic degradation of polylactic acid (PLA) and its composites" has been granted by Elsevier (License # 4776720538894)
- Permission to reproduce Table 2-2 which was published by Shady Farah in "Physical and mechanical properties of PLA, and their functions in widespread applications — A comprehensive review" has been granted by Elsevier (License # 4781000086195)
- Permission to reproduce Figure 1.1. which was published by Preetam Anbukarasu et al. in "A diffraction-based degradation sensor for polymer thin films" has been granted by Elsevier (License # 4776721109834)
- Permission to reproduce Figure 2.3, which was published by E. Castro-Aguirre et al. in "Poly(lactic acid)—Mass production, processing, industrial applications, and end of life" has been granted by Elsevier (License # 4776730591250)
- Permission to reproduce Figure 2.4, which was published by J. Ren, Biodegradable Poly(Lactic Acid): Synthesis, Modification, Processing and Applications, was granted by © Tsinghua University Press, Beijing and Springer-Verlag Berlin Heidelberg 2010 (License # 4776721354465)
- Permission to reproduce Figure 2.5, which was published by James Lunt in "Large-scale production, properties and commercial applications of polylactic acid polymers", has been granted by Elsevier LTD (License # 4776721466560)
- Thanks to Professor Victor Ugaz for his image of PLA degradation by proteinase K used in Figure 2.6, published in "A membraneless continuous-flow filter for high-throughput separation and enrichment of particles and cells", 14th International Conference on Miniaturized Systems for Chemistry and Life Sciences 3 - 7 October 2010, Groningen, The Netherlands, p. 873.
- Figure 2.7 was printed with the permission of Worthington Biochemical Corporation. The image was published in the website (http://www.worthington-biochem.com/introBiochem/effectspH.html)

- Permission to reproduce Figure 2.8 which was published in “Biological degradation of synthetic polyesters—Enzymes as potential catalysts for polyester recycling” by Rolf-Joachim Mueller, was granted by Elsevier (License # 4776760193717)
- Permission to reproduce Figure 2.9 that was published by Christopher Palmer and Erwin Loewen, in Diffraction Grating Handbook was granted by Newport Corporation.
- Permission to reproduce Figure 2.10, which was published by Dynasil Corporation in their website (https://www.dynasil.com/optical-materials/buyers-guide-to-selecting-a-diffraction-grating/), was granted by the company.
- Permission to reproduce Figure 2.11, which was published by Turan Erdogan on the Plymouth Grating Laboratory website (https://www.plymouthgrating.com/guidance/technical-notes/fundamentals/diffraction-efficiency), was granted by the author
- Permission to reproduce Figure 2.12 that was published by Donald O’Shea et al. in “Diffractive Optics: Design, Fabrication, and Test: Chapter 2” was granted by SPIE and by Professor O’Shea.

Appendix C: Troubleshooting

To evaluate the stability of PLA thin films with the diffraction-based setup is necessary to follow the next steps:

1. **Film casting**
    1. 1 gram of PLA pellets (sprayed with IPA) are dissolved in 200 mL of DMF at 120ºC until the pellets are completely dissolved and the solution is transparent (~30 min)
    2. Leave the solution to reach RT
    3. Leave the glass slides (with the PDMS mold) on the hotplate (at 110ºC) at least 5 min to reach the temperature before casting
    4. Cast 30 μL on top of the PDMS until the surface appears flat (~10 min) and count 30 seconds extra
    5. Remove from the hotplate and leave 1 week before peel off the films
2. **Film peeling**
    1. Spray IPA on the PLA films while they still are on top of the PDMS mold and let it dry
    2. Carefully place optical tape on top of the PDMS mold (with bigger size than the mold)
    3. Use heavy discs to fix the corners of the tape and two fine tweezers to be able to peel off the mold without cause wrinkles in the film
    4. Spay IPA and let it dry
    5. Choose the flattest area of the film and confirm the diffraction direction with a laser
    6. Cut the film to an approximate size of 1 cm × 0.5 cm and place it inside of a cuvette (previously rinse with IPA and completely dry)
3. **Enzyme solution**

The enzyme solution consists of 100 mg of proteinase K dissolved in 10 mL of storage buffer, distributed in aliquots of 0.5 mL kept at -20ºC.

1. The enzyme solution will change in concentration, temperature and pH.
2. Depending on these parameters, the buffer (with the corresponding pH) will be heated at the required temperature
3. For every experiment the enzymatic solution should be prepared at the moment

4. Take the corresponding amount and dissolve it in the adequate volume (in the optic lab right before start acquiring data)

4. Cuvette placement and laser alignment

1. The cuvette with only the PLA film, should be placed in front of the laser beam (inside the oil) and fixed with the tweezers
2. The laser beam diffracts when it hits the PLA film (at least 3 dots should be observed)
3. Align the sensor and fixed it in the corresponding positions (~10 mW when it is dry, ~1 mW when it is in the solution)
4. Check the reference beam, align and fix it (the approximate value should be ~4mW)

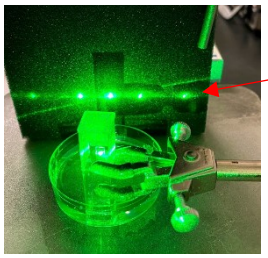

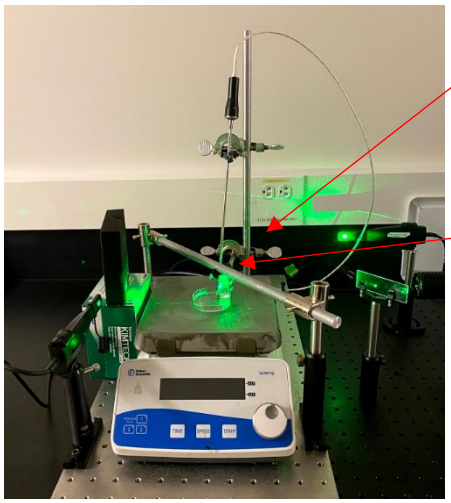

5. Software

1. Leave the laser ON (2.8 V) but close it to stabilize it (at least 5 minutes)
2. Using PowerMax software, review the sensor that it is going to be used and the wavelength parameters ($\lambda = 532\ nm$)
3. Check that every data point is acquired with a Time Interval of one second
4. Took 5 minutes of data without lights for both sensors: start putting Zero Sensor and press Log Data to File in ON

5. Review file name and location

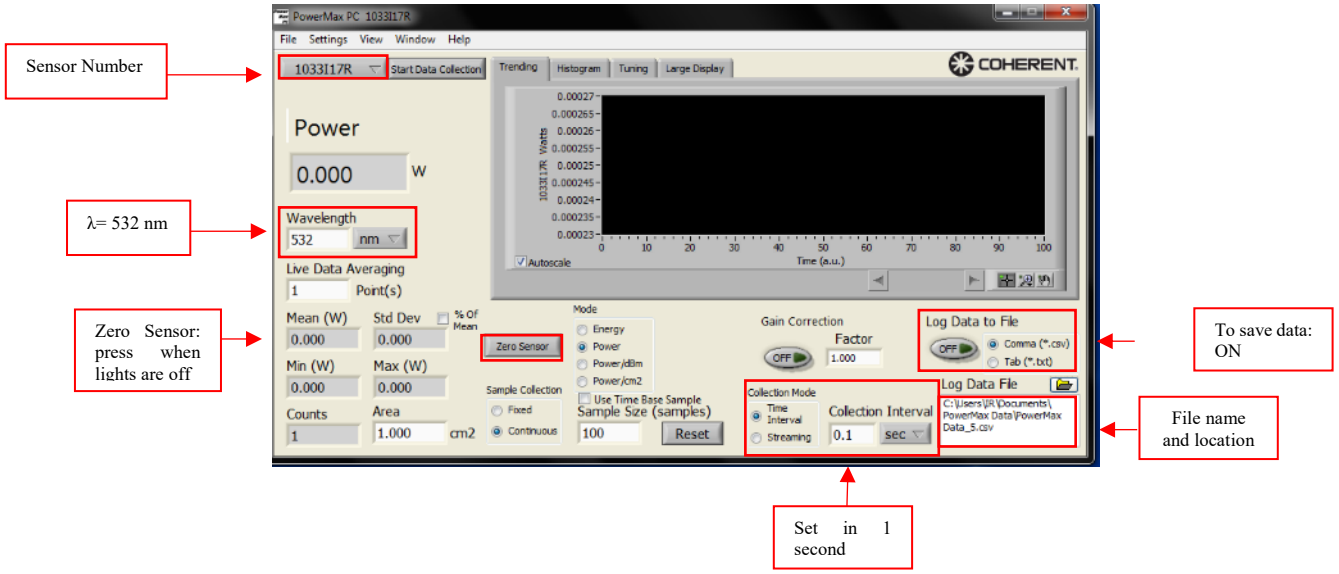

6. Diffraction setup

1. Due to heat differences, the hotplate should be set in the temperature according the next table. It requires ~30 min to reach the temperature

Desired temperature in the cuvette	Hotplate temperature
37ºC	44ºC
50ºC	63ºC
60ºC	73ºC

2. The oil container should have a stirrer to keep the oil temperature uniform, the revolutions per minute are 90
3. Once the cuvette is fixed and aligned, prepare the enzymatic solution and check that the temperature is the desired
4. Insert the solution in the cuvette and observe the drop in the software (from 10 to 1 mW)
5. Put a lid on the cuvette (previously sprayed with IPA and completely dry)
6. Fixed the lid using a small sponge and a transversal tube on top, fixed to the table
7. Review intensity values (once the film is in the solution the intensity is ~ 1 mW)
8. Change file name and press Log Data to File ON

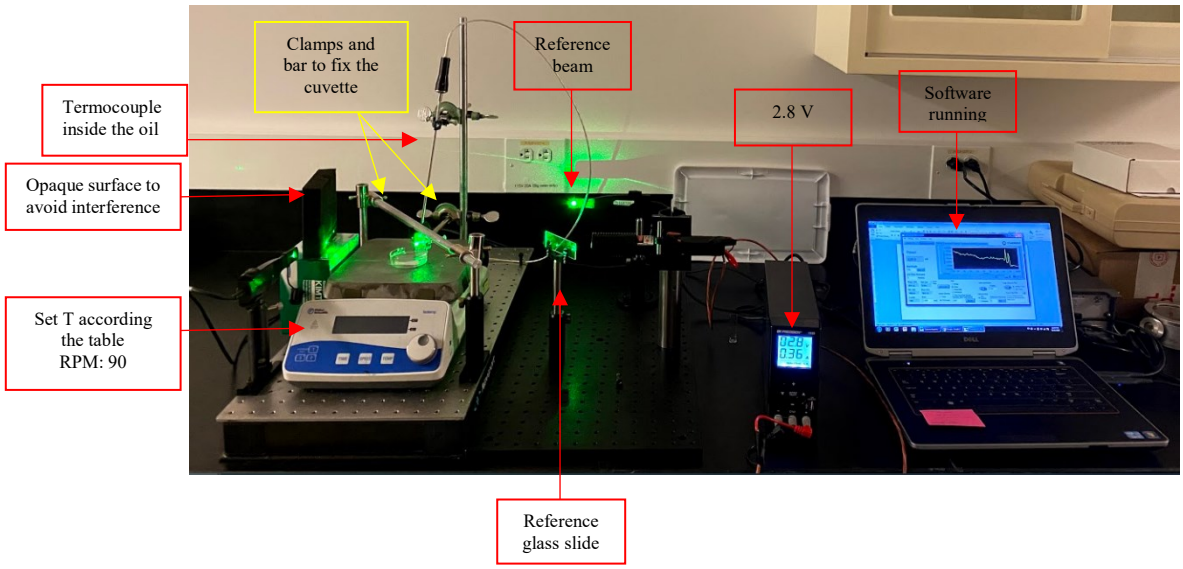
Clamps and bar to fix the cuvette
Reference beam
Termocouple inside the oil
2.8 V
Software running
Opaque surface to avoid interference
Set T according the table
RPM: 90
Reference glass slide